UNIVERSIDADE DE SÃO PAULO
FACULDADE DE FILOSOFIA, CIÊNCIAS E LETRAS DE RIBEIRÃO PRETO
PROGRAMA DE PÓS-GRADUAÇÃO EM FÍSICA APLICADA À MEDICINA E BIOLOGIA

"Miristoilação e seus efeitos na Proteína de Estruturação e Compactação do Golgi (GRASP)"

Emanuel Kava

Dissertação apresentada à Faculdade de Filosofia, Ciências e Letras de Ribeirão Preto da Universidade de São Paulo, como parte das exigências para obtenção do título de Mestre em Ciências, obtido no Programa de Pós-Graduação em Física Aplicada à Medicina e Biologia

Ribeirão Preto - SP

2021

UNIVERSIDADE DE SÃO PAULO
FACULDADE DE FILOSOFIA, CIÊNCIAS E LETRAS DE RIBEIRÃO PRETO
PROGRAMA DE PÓS-GRADUAÇÃO EM FÍSICA APLICADA À MEDICINA E BIOLOGIA

“Miristoilação e seus efeitos na Proteína de Estruturação e Compactação do Golgi (GRASP)”

Emanuel Kava

Dissertação apresentada à Faculdade de Filosofia, Ciências e Letras de Ribeirão Preto da Universidade de São Paulo, como parte das exigências para obtenção do título de Mestre/Doutor em Ciências, obtido no Programa de Pós-Graduação em Física Aplicada à Medicina e Biologia.

Orientador: Prof. Dr. Antonio José da Costa Filho

Ribeirão Preto - SP

2021

Ficha Catalográfica

Kava, Emanuel
Miristoilação e seus efeitos na Proteína de Estruturação e Compactação do Golgi (GRASP), Ribeirão Preto, 2021. 91 p.

Dissertação de Mestrado apresentada à Faculdade de Filosofia, Ciências e Letras de Ribeirão Preto/USP. Área de concentração: Física Aplicada à Medicina e Biologia

Orientador: Costa-Filho, Antonio José

1. Miristoilação 2. GRASP 3. Interação com membrana 4. Dinâmica molecular 5. Espectroscopia.

Dissertação de autoria de Emanuel Kava, sob o título "**Miristoilação e seus efeitos na Proteína de Estruturação e Compactação do Golgi (GRASP)**", apresentada ao Departamento de Física da FFCLRP-USP como parte das exigências para obtenção do título de Mestre em Ciências (Física Aplicada à Medicina e Biologia). Área de concentração: Física Aplicada à Medicina e Biologia, aprovada em 02 de agosto de 2021 pela comissão julgadora constituída pelos doutores:

Prof. Dr. Antonio José da Costa Filho

Instituição: Universidade de São Paulo

Presidente

Prof. Dr. Pietro Ciancaglini

Instituição: Universidade de São Paulo

Prof. Dr. José Luiz Lopes

Instituição: Universidade de São Paulo

I dedicate this work to my parents.

Acknowledgments

I am extremely grateful to all my friends who helped and taught me this new world of biological sciences. I am satisfied with all experiences I had in LBM lab, including parties, discussions and teachings with each one of you.

I am very grateful to my supervisor Antonio Jose da Costa Filho, I am sure that he was the right person to choose to guide me in this phase of my life, a sensitive and extremely smart guy. Thanks for giving me the opportunity to learn more and proud my family going too far from our reality.

Thanks to my lab friends: Ariane, Bruno, Carol, Dany, Fátima, Natália, Nathan, Pops and Thiru. All you know what we passed together, and I will always remember it affectionately.

Special thanks to my “mestres”, as I always mention them, Luis Felipe and Mariana Bunoro, who taught me and directed me to learn what I am going to present in this dissertation.

I am thankful to my great friends from Castro, Ponta Grossa, Curitiba and Joinville: Adriano, Rômulo, Renan, Pablo, Rhuan e Lukinhas. From music and poetry to science and philosophy, our discussions were extremely important.

Many thanks to Carolina, my girlfriend. No words to describe all our involvement and engagement.

I am very grateful to CAPES for its financial support over the years (grant no (88882.378790/2019-01). FAPESP and CNPq also were fundamental for the execution of this project.

*"*Science cannot solve the ultimate mystery of nature. And that is because, in the last analysis, we ourselves are a part of the mystery that we are trying to solve."

Max Planck

*(**Armchair Physics: From Electricity to Escape Velocities: The E = mc^2 of Everyday Life**. Isaac McPhee. New York: Chartwell Books, 2018.)*

"Sou um técnico, mas tenho técnica só dentro da técnica.
Fora disso sou doido, com todo o direito a sê-lo. Com todo o direito a sê-lo, ouviram?"

*(**Poesias de Álvaro de Campos**. Fernando Pessoa. Lisboa: Ática, 1944 (imp. 1993))*

Abstract

KAVA, Emanuel. **Myristoylation and its effects on the Golgi Reassembly and Stacking Protein (GRASP)**. 2021. 91 p. Dissertation (Master of Science) – Ribeirão Preto School of Philosophy, Sciences and Letters, University of São Paulo, Ribeirão Preto, 2021.

GRASP55 is a myristoylated protein localized in the medial/trans-Golgi faces and involved in the Golgi structure maintenance and the regulation of unconventional secretion pathways. It is believed that GRASP55 achieves its main functionalities in the Golgi organization by acting as a tethering factor and, when bound to the lipid bilayer, its orientation relative to the membrane surface is restricted to determine its proper *trans*-oligomerization. Despite the paramount role of myristoylation in GRASP function, the impact of such protein modification on the membrane-anchoring properties and the structural organization of GRASP remains elusive. Here, an optimized protocol for the myristoylation in *E. coli* of the membrane-anchoring domain of GRASP55 is presented. The biophysical properties of the myristoylated/non-myristoylated GRASP55 (residues 1-207) were characterized in a membrane-mimicking micellar environment. Although myristoylation did not cause any impact on the protein's secondary structure, according to our circular dichroism data, it had a significant impact on the protein's thermal stability and solubility. Electrophoresis of negatively charged liposomes incubated with the two GRASP55 constructions showed different electrophoretic mobility for the myristoylated anchored protein only, thus demonstrating that myristoylation is essential for the biological membrane anchoring. Molecular dynamics simulations were used to further explore the anchoring process in determining the restricted orientation of GRASPs in the membrane.

Keywords: Myristoylation. GRASP. Membrane interaction. Molecular Dynamics. Spectroscopy.

Resumo

KAVA, Emanuel. **Miristoilação e seus efeitos na Proteína de Estruturação e Compactação do Golgi (GRASP)**. 2021. 91 f. Dissertação (Mestrado em Ciências) – Faculdade de Filosofia, Ciências e Letras, Universidade de São Paulo, São Paulo, 2021.

GRASP55 é uma proteína miristoilada localizada nas faces medial/trans do Golgi, e com envolvimento na manutenção da estrutura do Golgi, bem como na regulagem de vias de secreção não-convencionais. Acredita-se que a GRASP55 realiza suas principais funções na organização do Golgi agindo como um fator de conexão, e quando ligada à bicamada lipídica, sua orientação em relação à superfície da membrana é restrita para determinar sua trans-oligomerização de maneira adequada. Apesar da importância da miristoilação na função da GRASP e no ancoramento em membranas, o impacto dessa modificação proteica nas propriedades de ancoramento e organização estrutural das GRASPs permanece elusivo. Neste trabalho, um protocolo otimizado para a miristoilação de GRASP55 em *E. coli* é apresentado, e os domínios de ancoramento miristoilado/não-miristoilado (resíduos 1-207) foram caracterizados através de suas propriedades biofísicas em um ambiente micelar. Apesar de a miristoilação não ter causado impactos na estrutura secundária, de acordo com os dados de dicroísmo circular, esta lipidação causou um grande impacto na estabilidade térmica e solubilidade proteica. A eletroforese de lipídeos negativamente carregados previamente incubados com as duas versões de GRASP55 apresentou uma mobilidade eletroforética diferente apenas para a proteína miristoilada, demonstrando que a miristoilação é essencial para o ancoramento em membranas biológicas. Simulações de dinâmica molecular foram utilizadas para explorar o processo de ancoramento determinação da orientação restrita das GRASPs na membrana.

Palavras-chave: Miristoilação. GRASP. Interação com membrana. Dinâmica molecular. Espectroscopia.

List of Figures

List of tables

Summary

1. Introduction

1.1. *Conventional and unconventional secretory pathways*

The majority of eukaryotic proteins are secreted to the extracellular medium through the most common secretory mechanism, known as the conventional secretory pathway, characterized by protein transport from the endoplasmic reticulum (ER) to the Golgi complex [1]. In this conventional pathway, secretory proteins depend on an internal or amino-terminal signal peptide for its translocation into the lumen of the ER, followed by a vesicular transport to the Golgi membrane [1].

Recently, integral membrane proteins that possess the signal peptide and proteins lacking the signal sequence (called leaderless proteins) have been shown to reach the cell surface via Golgi-independent pathways, which have been generally termed unconventional secretion pathways [2]–[5]. Until now, several unconventional mechanisms have been described [6], evidencing the considerable complexity involved in molecular transport and its regulation inside the cells. With rare exceptions, unconventional mechanisms are triggered by cellular stress caused by the lack of nutrients, inflammation, or mechanical stress [7].

The most common classification of unconventional protein secretion (UPS) encompasses four types of transport (**Figure** 1): direct secretion or pore-mediated translocation of the protein through the plasma membrane (type I); ABC-transporter-mediated secretion (type II); autophagosome/endosome-based secretion (type III), and leader-sequence containing transmembrane proteins synthesized in the ER and that bypass the Golgi in route to the plasma membrane (type IV) [6].

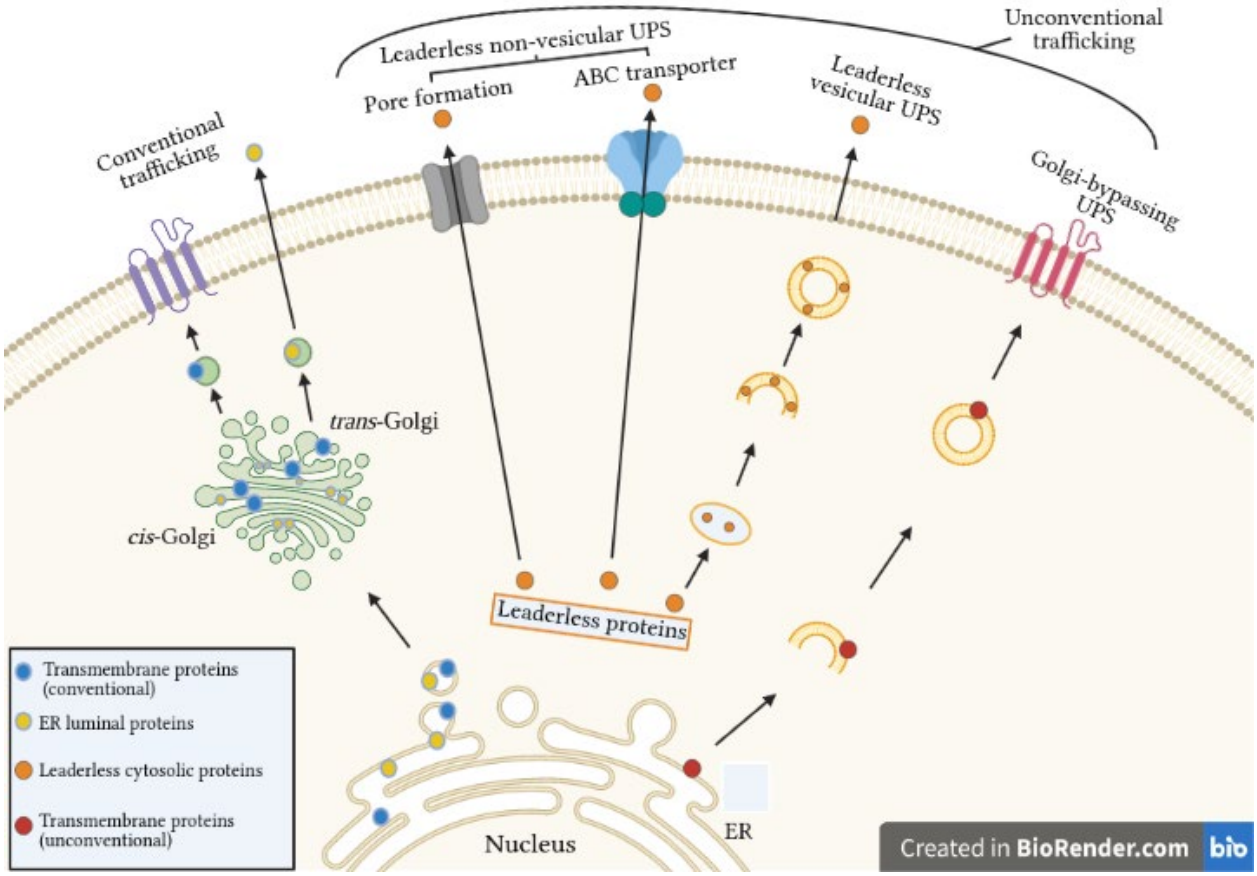

Figure 1 – Scheme of conventional and unconventional secretion pathways. The conventional secretion pathway is characterized by the ER-to-Golgi transport of cargo proteins (yellow and blue circles), which contain a leader sequence. The UPS types I and II involve transporting cytosolic proteins without a leader sequence (orange circles) through a membrane pore and the ABC transporter. UPS types III and IV involve the vesicular transport of leaderless cytosolic proteins and transmembrane proteins (red circles). Adapted from reference [7], created using BioRender (https://biorender.com/).

1.2. *The Golgi apparatus*

The Golgi complex is an organelle found in all eukaryotic cells, where it performs a central role in the exocytic pathway. The most well-known biochemical functions assigned to the Golgi complex are related to the transport and targeting of early synthesized proteins [8]. The Golgi is structurally arranged as laterally linked stacks of

cisternae, which give rise to a polarized organelle divided into *cis*, *medial,* and *trans* regions (**Figure 2**A) [9].

This arrangement is directly related to the post-translational modifications taking place in the Golgi when it receives proteins produced in the ER, such as N- and O-glycosylation [10], glycosaminoglycans synthesis [11], sulfation [12], and phosphorylation [13]. One interesting feature is seen in electron microscopy images of the Golgi in the proteinaceous bridges (**Figure 2**B) responsible for "gluing" the cisternae together in the stack [14].

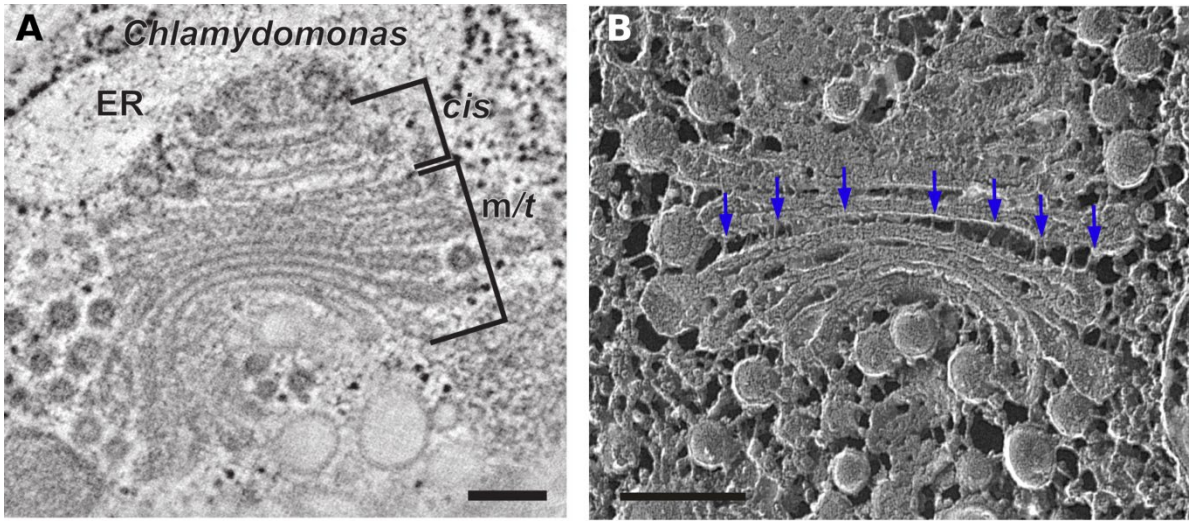

Figure 2 – (A) Tomographic slice image of Golgi stacks identifying the *cis* and *medial/trans* (m/t) regions. Adapted from reference [15]. (B) Electron micrograph of Golgi apparatus, showing the proteinaceous bridges (blue arrows). Images are from the green alga *Chlamydomonas inhartii,* and scale bars are = 100 nm. Adapted from reference [14].

1.3. *Golgi ReAssembly and Stacking Proteins (GRASPs)*

GRASPs are proteins firstly reported as Golgi stacking factors [16], [17]. In this structural role, GRASPs rely on the interaction with their respective golgin partners. For instance, in vertebrates, the two isoforms of GRASPs (GRASP65/GORASP1 and

GRASP55/GORASP2) form complexes with GM130 [18] and Golgin 45 [19], respectively. GRASP65 was first identified in the *cis* cisternae due to its sensitivity to the alquilant reagent NEM (N-ethylmaleimide) [16]. GRASP55 was also discovered through NEM reactivity two years later, identified as a homolog protein with a sequence identity of 66% located in the *trans-medial* cisternae [17]. GRASP orthologues and homologs have been identified in flies [20], yeast [21], and parasites [22]. Plants are an exception in this aspect since they do not possess any GRASP homologs but still maintain the flattened Golgi apparatus organized in stacked cisternae [23].

Since GRASP homologs in *Dyctyoselium* and *Drosophila* do not participate in Golgi organization but act in unconventional secretion, the role in cisternae structuration seems to be a later characteristic in the evolutive development of these proteins [24]. During the last few years, the exact function of GRASPs in organizing the Golgi structure has been a matter of intense debate [6], [25], [26]. GRASP single or double knockout models have been reported, giving controversial results regarding GRASP's role in the stacking function [27], [28]. More recently, a Golgi presenting reduced cross-sectional diameters of laterally disconnected cisternae has been described in a mouse lacking GRASP55 and GRASP65 [26].

In contrast to this debatable aspect regarding the Golgi organization, the participation of GRASPs in processes related to the unconventional secretion (types III and IV) of cargo has been firmly established [29]–[31]. For example, the GRASP homolog in *Dictyostelium* mediates the acyl-CoA binding protein (ACBP) transport and the transport of α-integrin in *Drosophila* in specific developmental stages through a Golgi-independent non-conventional route. The secretion of the pro-inflammatory cytokine interleukin 1β (1L-1β) is GRASP-dependent upon nutrient starvation in mammalian cells [32], [33]. GRASP's relocalization into the ER plays an essential role in the cell-surface trafficking of ΔF508-cystic fibrosis transmembrane conductance regulator (CFTR) [3], [34]. GRASPs are structurally formed by two main domains (**Figure 3**). The highly conserved GRASP domain (DGRASP) is myristoylated at the glycine 2 (Gly2) and anchored to the Golgi membranes [35]. The GRASP's golgin partners have a C-terminal peptide region that interacts at two different sites concurrently: the canonical

PDZ peptide-binding groove of the PDZ1 and additional residues on the PDZ2 surface or the region connecting both subdomains [36], [37]. The second domain of GRASPs is the intrinsically disordered SPR (Serine and Proline-rich), which has regulatory functions and is not conserved even among evolutionary close species [35].

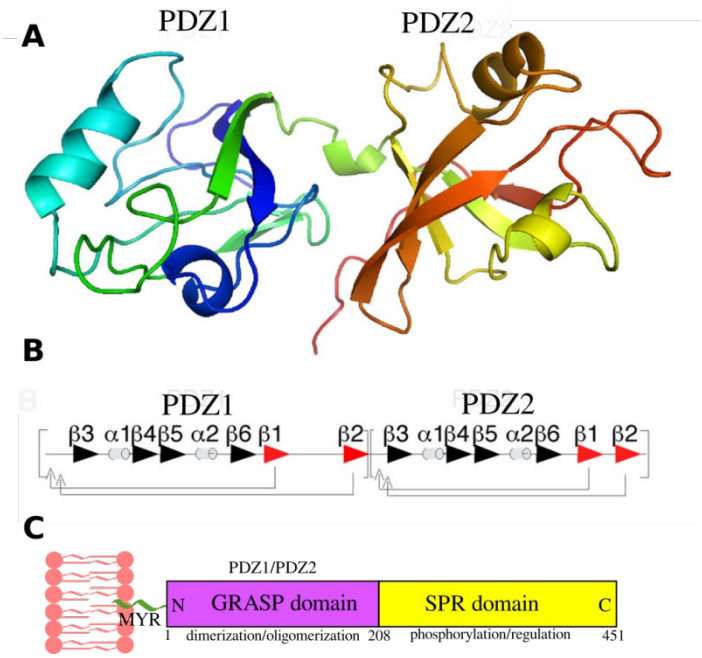

Figure 3 – (A) Structure of GRASP55 PDZ1 and PDZ2 domains (1-207) separated by a short α-helix. (B) Secondary structure representation of GRASP55 GRASP domain with a typical eukaryotic PDZ (PSD95/DlgA/Zo-1) domain. (C) Full-length human GRASP55 domains with a conserved myristoyl-anchored GRASP domain consisting of PDZ1 and PDZ2 subdomains and the C-terminal serine and proline-rich (SPR) domain. Figure adapted from references [38], [39].

GRASPs interact with several proteins while performing their functions [40], evidencing their structural plasticity. For example, GRASP55 participates in autophagosome/lysosome fusion in the absence of glucose, acting as a bridge between the proteins LC3 and LAMP2. This function is regulated through the post-translational N-acetylglucosamination, thus facilitating autophagosome maturation [25]. GORASP2 knockout leads to defects in mouse spermatogenesis, causing infertility, affecting GRASP55 interaction with JAM-C through a binding motif in PDZ domains [41]. The GRASP interaction with several members of the cargo receptors p24/TMED family,

which are transmembrane components of vesicles recycling between the ER and the Golgi complex, facilitates the conventional protein secretion pathway [42]. Interaction between GRASP55 and the Transforming growth factor-α (TGF-α) plays an important role in the maturation and transport of TGF-α through the Golgi [43]. CD83, a membrane protein expressed in mature dendritic human cells, specifically interacts with GRASP55, showing a functional role in cell maturation [44]. GRASP55 also acts as a molecular bridge between the membrane-type 1 matrix metalloproteinase (MT1-MMP) and furin [45].

1.4. The role of GRASPs in Golgi structure

Despite the debate on the precise role of GRASP in the Golgi structure, a considerable amount of data has been produced proposing structural models that could account for that role. GRASPs are peripherally membrane proteins anchored to the Golgi through myristoylation in Gly2 and the interaction with the respective coiled-coil golgin [27], [46], [47]. The membrane anchoring has given GRASPs a multitask tethering function observed *in vitro* and *in cell*-based assays [26]. The data reported so far indicate that tethering occurs via the *trans*-oligomerization of the PDZ domains in juxtaposed vesicles [26], [48], [49]. During mitosis, phosphorylation of GRASP65 by kinases Cdk1 and Plk1 leads to the disassembly of the oligomers and cisternae unstacking, and the post-mitotic dephosphorylation by PP2A causes re-oligomerization [50]. According to Truschel *et al.* (2013), the GRASP55 GRASP domain (DGRASP55) forms a homodimer through binding of the PDZ2 of one GRASP molecule with the PDZ1 of the opposed protein [38]. In a second proposed model, the homodimer is formed by a PDZ2 binding pocket-mediated interaction only [49]. The crystal structure determination of the DGRASP55 complexed with the Golgin45 C-terminal peptide led Zhao and colleagues [37] to propose a GRASP55 oligomerization model in the *mid*-cisternae (**Figure 4**).

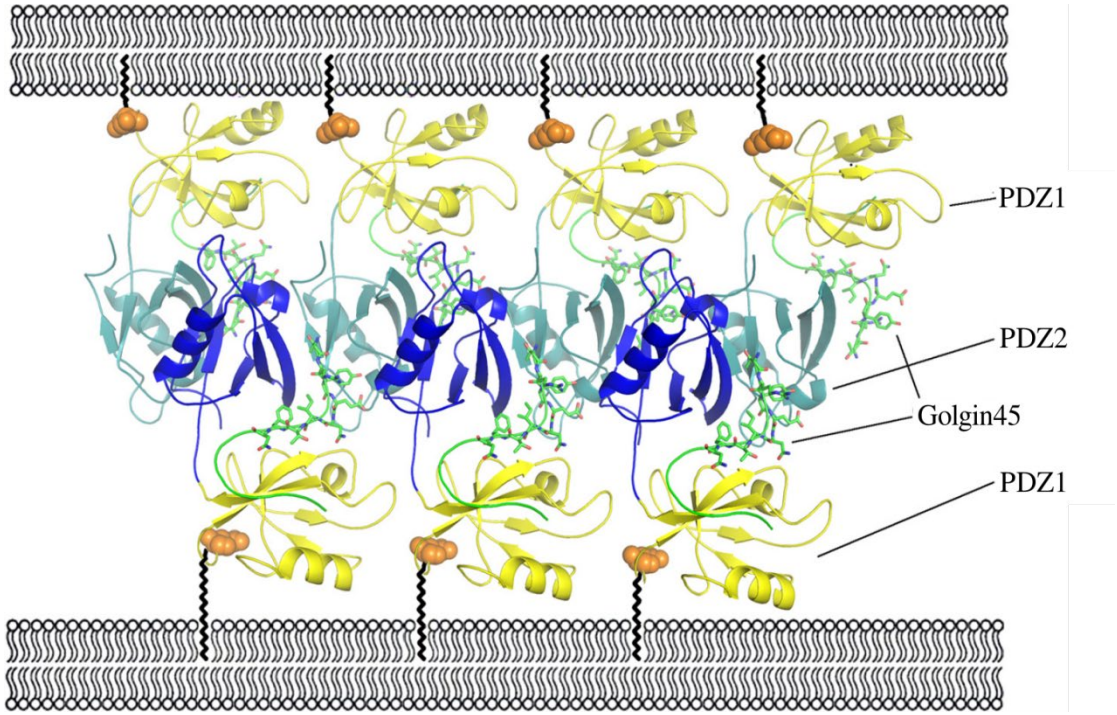

Figure 4 – Model of the GRASP55 oligomerization between Golgi cisternae membrane proposed by Zhao *et al.* (2017). The orange and the zigzag represent the N-terminal myristoylation, while PDZ1 and PDZ2 are colored in yellow and blue, respectively. Green sticks represent the C-terminal peptides of Golgin45. Figure adapted from reference [37].

One major limitation in all those models of GRASP oligomerization is that they were based on the crystal structures of the GRASP domain obtained without the N-myristoylation. The lack of this modification is likely to have an impact on findings related to GRASP-membrane interaction. For example, unlike the expected dimer configuration in the Golgi, the non-myristoylated version of DGRASP55 has already been shown to behave predominantly as monomers in solution [51], [52]. Furthermore, the depletion of mammalian GRASPs led to the loss of the golgins GM130, p115, and Golgin-45 from the Golgi, suggesting that GRASPs are indeed responsible for anchoring golgins, and not the opposite [26]. Therefore, we can conclude that the role of the N-

myristoylation in GRASP structure and function has been underappreciated in previous studies.

1.5. *Protein lipidation*

Proteins can be modified with the covalent attachment of lipids in the cytoplasm, cytoplasmic membrane face, or in the lumen of the secretory pathway [53]. Protein lipidation involves amides [i.e., N-α-myristoylation (MYR) and glycosylphosphatidylinositol (GPI) anchors], thioesters [i.e., S-palmitoylation (PAL)], and thioethers (i.e., isoprenylation and farnesylation) [53]. MYR, PAL, and prenylation are common lipidations that occur in the cytoplasm [53]. GPI anchor is the best-characterized lipid modification occurring in the lumen of the secretory pathway [54]. These processes affect, for instance, the charge and the hydrophobicity of the modified molecule, therefore resulting in physiologically relevant changes [55]. Such modifications occur in many eukaryotic proteins and act as regulators of several biological pathways: protein secretion, membrane trafficking, signal transduction, and apoptosis [56]. Effects of lipidation include regulating protein-membrane interactions, protein-protein interaction, protein stability, and enzymatic activities [56].

The lipidation processes can occur at the nucleophilic protein side chains (in lysines, cysteines, and serines) and the N-terminal amino (NH_2) group. GPI anchoring [54] and cholesterol esterification [57] are examples of C-terminal lipid modifications. **Figure 5** represents the diversity of protein lipidations so far known.

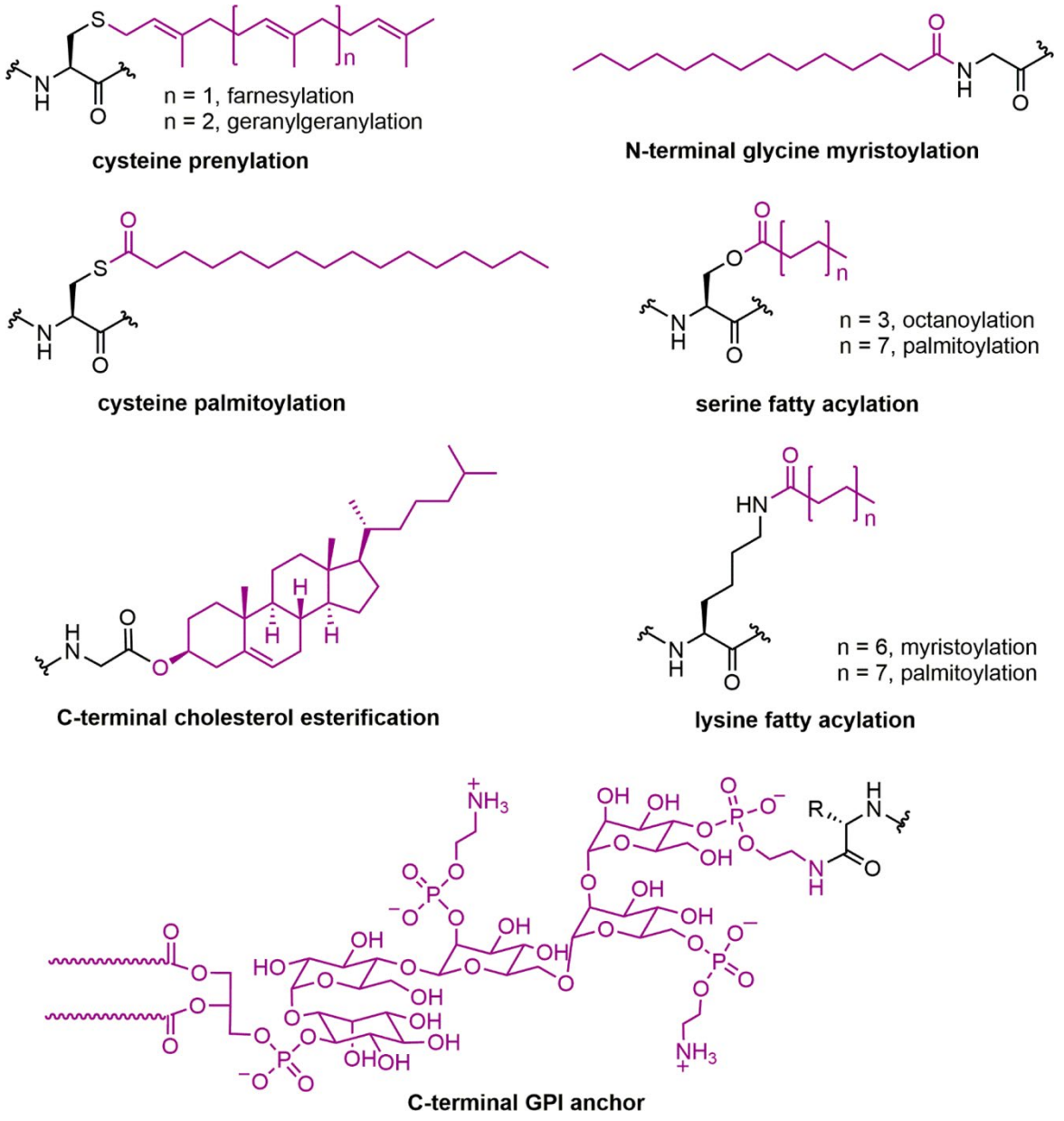

Figure 5 – Protein lipid modifications. Figure adapted from reference [56].

1.5.1. Myristoylation

The N-myristoylation is a fatty acylation at Gly or Lys residues, which occurs co-translationally after the cleavage of the initial methionine by methionylaminopeptidases [58] or post-translationally upon the exposure of a 'hidden' myristoylation site upon cleavage by specific proteases [59]. It is catalyzed by N-terminal myristoyltransferases (NMTs), which are members of the GCN5-related N-acetyltransferases (GNAT) family [60]. In humans, the transfer of the myristate group to the N-terminal glycine is performed by NMT1 and NMT2, being NMTs responsible for the myristoylation of about 2% of any eukaryotic proteome [61], when considering NMTs sequence recognition pattern. Recently, mapping of myristoylation in several proteins resulted in the first description of what has been called the myristoylome, the first lipidated proteome [61], [62].

The emergence of NMTs is linked to eukaryogenesis, and therefore myristoylation does not happen in prokaryotes [61]. This lipidation contributes to the regulation of signaling and trafficking processes and is an essential mechanism for cell compartmentalization during the history of life [63]. Several signals control the reversible membrane interaction of myristoylated proteins, such as charge [64], [65], hydrophobicity [66], [67], and ligand interaction [68], [69], causing dissociation/association from the bilayer. For instance, the regulation signals involve the hydrolysis of GTP, which induces conformational changes affecting the myristate region [70], Ca^{2+} concentration dependence [71], [72], phosphorylation inducing electrostatic interactions with membrane phospholipids [73], or depalmitoylation of cysteine residues [74] located next to the myristate.

In the specific case of GRASPs, Heinrich *et al.* (2014) exploited the aspects of this lipidation in DGRASP55 orientation relative to the lipid bilayer surface. There, the authors used a strategy involving the double anchoring of the protein to the membrane induced by the Gly2 myristoylation and the interaction of a 6-His tag located in the C-terminus of myr-DGRASP55 with a 1,2-dioleoyl-sn-glycero-3-[(N-(5-amino-1-

carboxypentyl)iminodiacetic acid)succinyl] phospholipid inserted in the model membranes (**Figure 6**). As a result, the authors observed a GRASP domain-mediated membrane tethering and the stabilization of such interaction via the myristoylation. Moreover, the propensity for homotypic protein-protein interaction in *trans*, preventing *cis* interactions, was also reported.

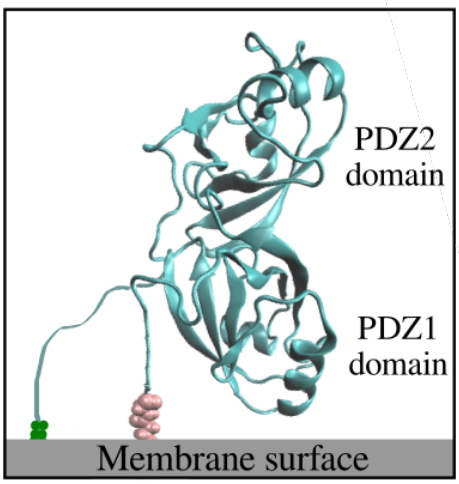

Figure 6 – myr-DGRASP55 orientation relative to the membrane surface modeled based on neutron reflection experiments. The myristoyl group is represented by pink spheres and the Ni^{2+}-ligated His tag by green balls. Figure adapted from reference [75].

2. Objectives

The data available hitherto in the literature and discussed in the previous section clearly indicate that the role of myristoylation in GRASP's function has been underappreciated. The great majority, if not all, studies reporting structural characterizations of GRASPs used constructions without that chemical modification. Thus, we only have a partial description, for instance, of the docking and trans-oligomerization of GRASPs with the effects of N-myristoylation not yet fully considered [75].

Therefore, the objectives of this dissertation focused on the structural aspects and the influence of this crucial fatty acylation in one member of the GRASP family, GRASP55. The lack of the N-myristoylation at Gly2 in previous reports was likely due to the use of recombinant DGRASPs expressed in *E. coli* and the challenge of working with membrane-bound proteins. These points explain why, despite the known importance of myristoylation for GRASPs, the impact of this lipidation on the GRASP structural behavior has still not been adequately addressed. Here, we described an optimization of the expression and purification protocol of the myristoylated GRASP55 GRASP domain (myr-DGRASP55) in *E. coli* and a biophysical characterization of this membrane protein so as to compare it with its soluble version (DGRASP55). Our data illustrated how myristoylation affects GRASP55 membrane anchoring tendency and structural stability with a clear impact on this protein propensity for oligomerization. To accomplish this general objective, the following specific goals were pursued:

- ✓ Optimization of the myristoylation protocol reported by [76]
- ✓ Expression and purification of the myr-DGRASP55
- ✓ Structural characterization of myr-DGRASP55 using experimental methods, such as circular dichroism
- ✓ Structural characterization of the non-myristoylated version of DGRASP55 using the same methods, thus allowing us to perform the respective comparisons
- ✓ Investigation of the interaction between the membrane models and DGRASP55 or myr-DGRASP55 using molecular dynamics simulations

3. Materials and Methods

3.1. *Protein expression and purification*

The gene encoding DGRASP55 was amplified with One Taq® DNA Polymerase (New England BioLabs) from a previous plasmid available in our group [77] using the primers DGRASP55F (5'-CATGATCCATGGGCTCCTCGCAAAGC-3') and DGRASP55R (5'-CATGATCTCGAGCTCAAATGGGCGTG-3'). For PCR, the parameters were set as 94 °C for 30 s, followed by 30 cycles of 94 °C for 30 s, 55 ºC for 30 s, 72 ºC for 1 min, and final incubation at 72 ºC for 10 min. The digestion of the PCR product was done with XhoI and NcoI and cloned into the plasmid pET-28a-c(+). This way, the HisTag in the N-terminal in the template plasmid used in [77] was changed to the C-terminal. The ligation reaction was done with T4 DNA Ligase (New England BioLabs). The final construct (pET28a-DGRASP55) was transformed into DH5α *Escherichia coli*, purified with the kit Wizard SV gel and PCR clean-up system (Promega), and sequenced in the Hemocentro of Hospital das Clínicas (FMRP-USP). *E. coli* Rosetta (DE3) cells (Novagen, Darmstadt, Germany) were transformed with the resulting vector pET28a-DGRASP55 and grown at 37 ºC and 200 rpm agitation until reaching an OD (Optical Dispersion) of 0.8 in LB medium supplemented with 50 mg/L kanamycin and 34 mg/L chloramphenicol. For the myristoylated protein expression, the DGRASP55 and CaNMT1-pET-22b(+) plasmids were co-transformed in *E. coli* Rosetta strain, grown in LB medium supplemented with 50 mg/L kanamycin, 34 mg/L chloramphenicol and 100 mg/L ampicillin. The expression was carried out for 18 h, induced with 0.5 mM isopropyl β-D-thiogalactopyranoside (IPTG) at 18 ºC and 200 rpm agitation. For myr-DGRASP55 expression, myristic acid (250 μM), previously solubilized in ultrapure ethanol, was added to the cell solution together with the IPTG. Cells were harvested at 7,000x g for 10 min and resuspended in 20 mL of lysis buffer (20 mM Tris/HCl pH 8.0, 150 mM NaCl, 1% Triton X-100) per liter of cell culture. The cell disruption by sonication was done in a Branson 450 Digital Sonifier® (Sonitech), in ice at 48 x 5 s bursts, with an amplitude of 18% and a 15 s interval between bursts, followed

by centrifugation (12,000xg, 25 min) to separate the insoluble fraction. The supernatant was loaded into a 4 mL Ni^{2+}-NTA affinity column (Promega – Madison, USA), previously equilibrated with lysis buffer. After that, the nickel column was washed with 20 mL of buffer A (20 mM Tris/HCl pH 8.0, 0.03% DDM, 150 mM NaCl) with a crescent imidazole gradient (10 mM and 20 mM) to remove weakly bound contaminants in the resin. The protein was eluted with 10 mL of buffer A containing 350 mM imidazole. The resulting solution was concentrated with an Amicon Ultra-15 Centrifugal Filter (NMWL of 10 kDa, Merck Millipore, Burlington, MA, USA) and loaded into a Superdex200 10/300 GL gel filtration column (GE Health-care Life Sciences) coupled to an *Äkta purifier* system (GE Healthcare). The expression and purification of the eGFP tagged DGRASP55 (DGRASP55/pWALDO-d) followed the same protocol. To perform the subsequent experiments, we collected samples of DGRASP55 eluted in 16 mL to 17 mL and myr-DGRASP55 eluted from 15 mL to 17 mL. For protein concentration determination, the extinction coefficient at 280 nm was calculated with ProtParam web server [78], resulting in ε_{280}= 26,930 $M^{-1}.cm^{-1}$ and Abs 0.1% (= 1 mg/mL) of 1.183.

3.2. *Detergent adsorption*

The removal of DDM in the protein solutions was done by fixing the protein concentration at 1 mg/mL and using 30 mg of BioBeads SM2 (Bio-Rad, CA) per mg of protein. Then, the adsorbent was incubated with purified samples for 30 minutes at 4 ºC while shaking, followed by centrifugation (13,600xg per 1 minute).

3.3. *Circular Dichroism (CD)*

CD experiments were performed in a Jasco J-815 CD Spectrometer (JASCO Corporation, Japan) equipped with a Peltier temperature control, using a quartz cell with 1 mm path length for far-UV and 1 cm path length for near-UV. The scanning speed was 50 $nm \cdot min^{-1}$, a spectral bandwidth of 1 nm, a response time of 0.5 s, and averaging the

spectra using 9 different accumulations. The buffer solution was 20 mM of Sodium Phosphate buffer, pH 8.0, 0.03% DDM for far-UV measurements, and 20 mM Tris/HCl, 0.03% DDM, 150 mM NaCl, pH 8.0 for the near-UV. Protein concentration was 0.15 mg/mL for far-UV and 1.5 mg/mL for near-UV.

3.4. *Fluorescence spectroscopy*

Steady-state fluorescence was monitored using a Hitachi F-7000 spectrofluorometer equipped with a 150 W xenon arc lamp. The excitation and emission monochromators were set at a slit width of 5 nm in all experiments. The tryptophan excitation wavelength was set at 295 nm, and the emission spectra were measured from 310 up to 450 nm. Fluorescence quenching using the water-soluble acrylamide as a quencher was performed in a serial dilution from a 4 M acrylamide stock solution. The relation between the quencher concentration [Q] and the fluorescence intensity (I) was calculated through the Stern-Volmer relationship $I/I_0 = 1 + K_{SV}[Q]$, where I_0 is the fluorescence intensity in the absence of the quencher and K_{SV} the Stern-Volmer constant. The protein concentration was fixed at 15 μM, the buffer used was and 20 mM Tris/HCl, 0.03% DDM, 150 mM NaCl, pH 8.0 and all the fluorescence assays were performed at 25°C, after 5 minutes of thermal equilibration.

3.5. *Liposome preparation*

Lipids 1,2-dimyristoyl-sn-glycero-3-phosphocholine (DMPC); 1-palmitoyl-2-oleoyl-sn-glycero-3-[phospho-rac-(1-glycerol)] (POPG); 1,2-dimyristoyl-sn-glycero-3-phospho-(1′-rac-glycerol) (DMPG); Heart Polar Lipid Extract (Bovine); L-α-Phosphatidylethanolamine-N-(lissamine rhodamine B sulfonyl) (Ammonium Salt) (Egg-Transphosphatidylated, Chicken) (Egg Liss Rhod PE) were all purchased from Avanti Polar Lipids, Inc. (Alabama, U.S.A). The necessary quantity of phospholipids solubilized in chloroform was poured in glass tubes and slowly dried with nitrogen gas for liposome

preparation. An additional drying step was performed using a SpeedVac™ concentrator (SAVANT™) for 2 hours. The lipid film was resuspended in buffer A without DDM, and three cycles of freeze-thaw procedure was done to disrupt multilamellar vesicles. Large unilamellar vesicles (LUVs) were prepared by submitting the freeze-thawed vesicles to an extruder with a 100 nm pore size polycarbonate membrane from Whatman (Schleicher & Schuel). The liposomes were prepared in a 4 mM stock solution supplemented with 1% Egg Liss Rhod PE.

3.6. *Liposome electrophoretic mobility shift assay (LEMSA)*

Liposome electrophoresis was carried in a horizontal setup in a Tris-acetic acid (TAE) solution, and the agarose gel was made in a concentration of 0.35%. The lipid samples (200 μM) were pre-incubated with protein (20 μM) and supplemented with 5% glycerol. The voltage utilized was constant (75 V) at room temperature (20 ºC – 25 ºC). The relative electrophoretic mobility of myristoylated and non-myristoylated proteins was estimated utilizing the expression: $\mu = d(t)/Et$, where d(t) represents the distance measured from the start running point at time t, and E is the electric field used in the experiment. The image data was edited in the Inkscape software to enhance the contrast between the fluorescent bands and the background.

3.7. *Molecular Dynamics (MD) simulations*

All-atom Molecular Dynamics simulations were performed using the crystallographic structure (3RLE) of the GRASP55 GRASP domain from *Homo sapiens* (residues 7-208). The model of the missing N-terminal was generated by homology with Swiss model [79] with the PDB 5GML, the structure of the GRASP55 GRASP domain from *Mus musculus* with N-terminal extra residues. The CHARMM-GUI [80] web interface was used to generate an initial setup of the protein, the hydrated palmitoyl-oleoyl-phosphatidylcholine (POPC) or palmitoyl-oleyl-phosphatidylglycerol (POPG)

bilayer with 382 lipids units and 34,950 water molecules. To neutralize the system, $Na^{+}Cl^{-}$ ions were explicitly added. Simulations were performed with the NAMD package [81], CHARMM36 force-field [82], and TIP3P model for water. The PME method was used for long-range electrostatic interactions and a cutoff of 12 Å for van der Waals forces. The isothermal-isobaric ensemble at 303.15 K, 1 atm, and a time-step of 2 fs, was temperature-controlled by Langevin dynamics with 10 ps^{-1} for damping coefficient. For pressure control, the Nosé-Hoover algorithm with 200 fs of oscillation period and 100 fs for decay rate. Residue contacts (cutoff of 3 Å) and minimum distances, we utilized the software CPPTRAJ [83]. Trajectories were visualized using the VMD package.

4. Results

4.1. *Cloning of the DGRASP55 encoding gene*

The human DGRASP55 gene flanked by NcoI/XhoI restriction enzymes sites was amplified from an N-terminal 6xHis-tagged pET-28a(+)-DGRASP55 expression vector by using appropriate oligonucleotides. The PCR reaction resulted in products purified by selecting the corresponding gene band from 1% agarose gel electrophoresis (**Figure 7**). Next, the purified 621 bp fragment was ligated into the pET-28a(+) vector, previously linearized with the same restriction enzymes to form the construct. These steps were necessary to place the His-tag in the C-terminal region because the enzyme NMT from *Candida albicans* (CaNMT) requires a glycine in position 2 to perform the myristoylation. The resulting plasmids were propagated in *E. coli* DH5α, extracted, and confirmed by automated DNA sequencing.

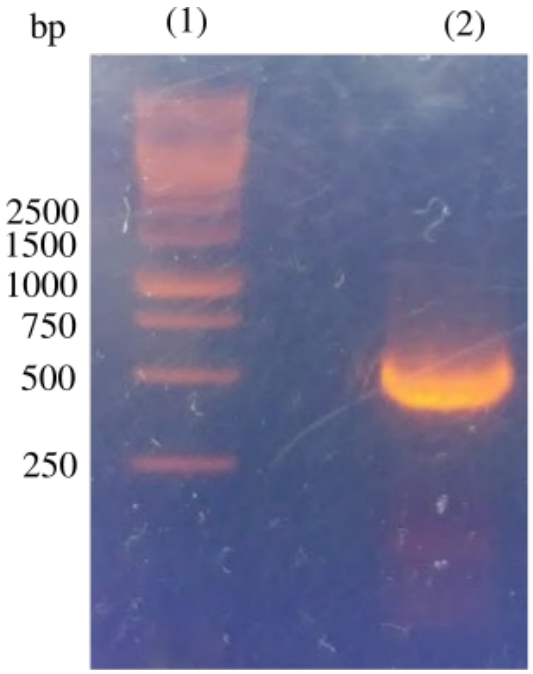

Figure 7 – Purified extract of the PCR amplification product of DGRASP55 encoding gene. (1) corresponds to GeneRuler 1kb DNA Ladder (Promega) and (2) amplified DNA fragment. Source: prepared by the author.

4.2. *Myristoylation of GRASP55*

We started by optimizing a previously described protocol used for the myristoylation of GRASP65 [76]. We decided to change the yeast NMT1 gene used in that previous report [76] for the well-characterized NMT cloned from *Candida albicans* (CaNMT), a stable protein with high activity and solubility [84]. CaNMT was cloned in a pET22b vector using the Nde1/Xho1 restriction sites, yielding a protein lacking any affinity tag. The CaNMT-pET22b (ampicillin-resistant) and the His-tagged DGRASP55-pET28a (kanamycin-resistant) were co-transformed in Rosetta (DE3). Cells were IPTG induced in the presence of 250 μM of either myristic acid or non-purified chemically synthesized azido-tagged analog of myristic acid (ω-Azido undecanoic acid) as described for the myristoylation protocols in [85]. We were not able to detect differences in efficiency between those reagents (data not shown). The ω-Azido undecanoic acid was kindly shared by Giuliano Clososki's lab (FCFRP – USP). The overexpression performed for 18 h at 18 ºC also helped to increase the total amount of well-folded protein. The results of the purification steps are shown in **Figure 8**.

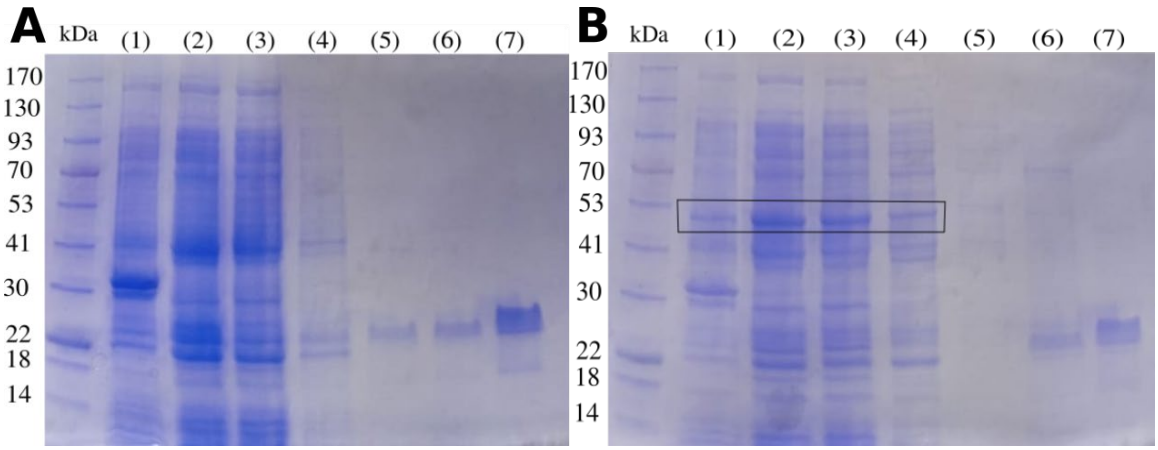

Figure 8 – (A) DGRASP55 and (B) myr-DGRASP55 purification in Ni^{2+}-NTA resin, visualized through SDS-PAGE; corresponding bands to CaNMT1 are highlighted by the black rectangle: (1) pellet after lysed cells centrifugation, (2) supernatant (lysate), (3) void (not bound to the column), (4) 20 mL washing buffer (Tris 20 mM, NaCl 150 mM, β-Mercaptoethanol 5 mM, DDM (0,03%) + imidazole 10 mM, (5) 20 mL washing buffer + imidazole 20 mM, (6) protein elution with 10 mL buffer + imidazole 350 mM, (7) fraction collected after gel filtration purification (Superdex200). Source: prepared by the author.

The success of the myristoylation protocol was indirectly checked by qualitatively evaluating the protein solubility after removing the detergent from the purified myr-DGRASP55 solution using the adsorbent Bio-Beads SM2. To do so, we expressed a version of DGRASP55 with an eGFP-tag in its C-terminus (DGRASP55/pWALDO-d). **Figure** 9 shows that the protein precipitated after removing the detergent, as highlighted by the green color of eGFP in the insoluble fraction after centrifugation. The control solution using the non-myristoylated DGRASP55 was shown to have its solubility utterly independent of the detergent's presence or absence. The non-polar polystyrene beads have a high surface area that adsorbs organic compounds from aqueous solutions [86]. When caught by the Bio-Beads, the detergent micelles expose the myristoyl chain that was previously surrounded by detergent, thus leading to protein aggregation. This result suggests that the myristoyl chain in DGRASP55 was already exposed to the aqueous environment and did not seem to need a switch mechanism to bring it outwards, as previously observed in other proteins [64], [87].

Figure 9 - Images showing the results of removing the detergent on the solubility of purified eGFP-tagged myr-DGRASP55 and DGRASP55. Source: prepared by the author.

4.3. *Myr-DGRASP55 and DGRASP55 behavior in solution*

The protein samples produced following the protocols whose results were shown in the previous sections were then analyzed using size exclusion chromatography (SEC). The DGRASP55 chromatogram was similar to those already presented in previous reports of DGRASPs [88]. On the other hand, the SEC elution profiles of myr-DGRASP55 covered a broader volume range than DGRASP55 (**Figure 10**A). In particular, a greater intensity of the peak corresponding to the column void volume was obtained (approximately 30% of the total column volume, ~ 7,2 mL [89]), hence suggesting lower solubility (**Figure 10**A). We also observed considerable amounts of aggregated protein when performing SEC of myr-DGRASP55 in the absence of DDM since the peak at the void volume in the chromatogram was more intense than the other elution peaks (**Figure 10**B). The samples collected here were submitted to SDS-PAGE,

whose results were shown in the previous section. In SDS-PAGE, DGRASP55 and myr-DRASP55 presented similar molecular masses and purity (**Figure** 8).

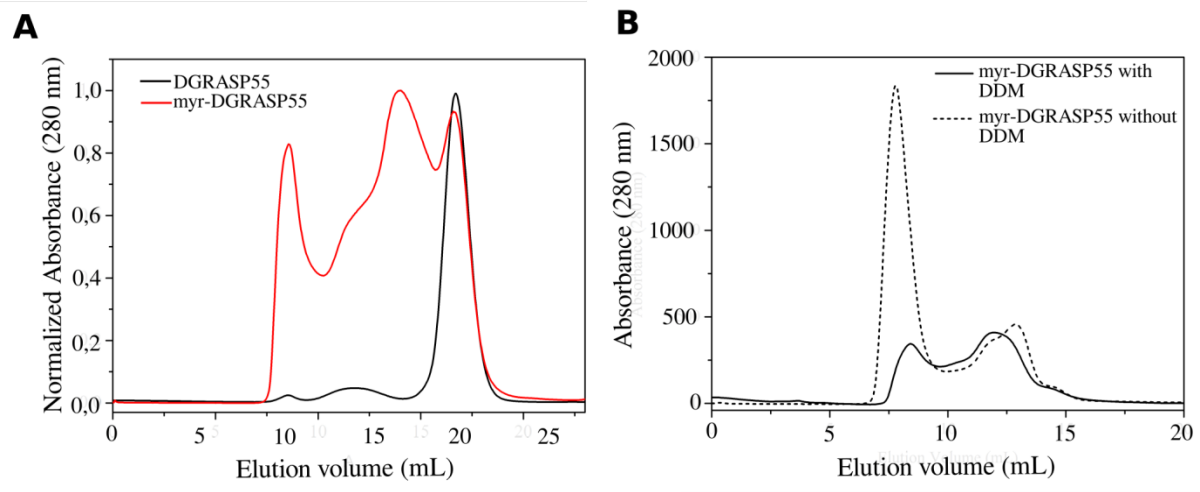

Figure 10 – Size exclusion chromatography of (A) myr-DGRASP55 and DGRASP55 in Superdex200 and (B) myr-DGRASP55 chromatogram in buffer with and without detergent in Superdex75. Source: prepared by the author.

Once the myristoylated construction was successfully expressed, purified and the presence of the myristoyl modification demonstrated, we then moved our attention to performing a more detailed biophysical characterization of the protein under investigation. To do so, we firstly performed circular dichroism experiments to assess potential changes in the protein's secondary structures and their spatial arrangements. The far-UV CD spectra of both proteins (**Figure 11**) were identical, evidencing that the myristoylation did not impact the secondary structures as monitored by the ellipticity in the far-UV wavelength region (198 nm – 260 nm). The spectra followed a similar profile observed in previous reports of DGRASP55 from our group [77].

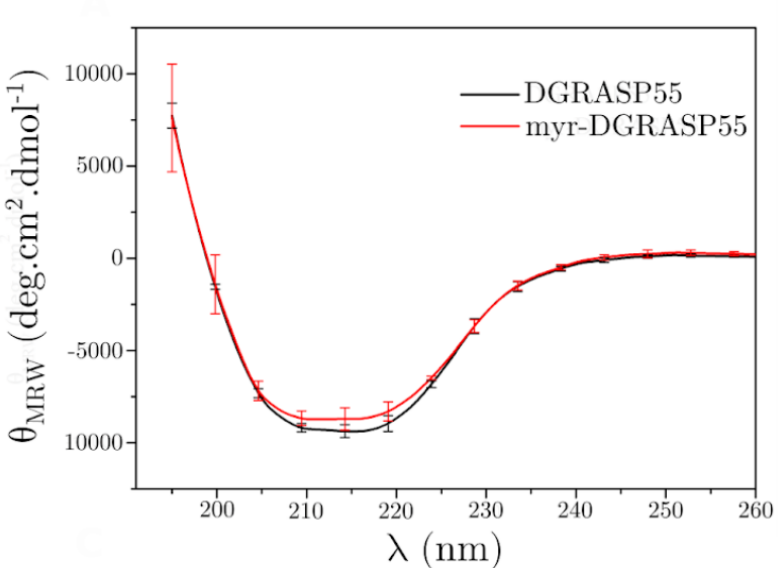

Figure 11 – Far-UV CD spectra of DGRASP55 and myr-DGRASP55. Source: prepared by the author.

Although the far-UV CD spectra of the myr-DGRASP55 and DGRASP55 were indistinguishable, their thermal unfolding followed different pathways (**Figure 12**). While the DGRASP55 spectra transitioned from the regular far-UV CD spectrum of ordered proteins to a spectrum typical of disordered structures, the myr-DGRASP55 spectra did not present significant changes, suggesting only a slight impact on the protein secondary structure. The structural organization induced by the myristoylation of the DGRASP55 seems to give rise to a more thermal stable protein, at least in terms of maintaining its secondary structure arrangement.

We again used circular dichroism experiments to explore further changes caused by the myristoylation, but now in the near-UV range. Unlike the far-UV data, the near-UV CD data showed significant differences between both versions of DGRASP55 (**Figure 13**A). This is because the near-UV CD detects the optical activity of aromatic residues (Trp, Phe, and Tyr), and the intensities observed are dependent on the environment around those aromatic side chains [90]. Since there were no significant changes in the secondary structure organization monitored by the far-UV CD, the

differences in the near-UV region were likely due to the alterations in the local environment of the aromatic residues in a region close to the myristoylation site.

To have more information on the changes around the aromatic residues seen in the near UV-CD spectra of myr-DGRASP55, we also used steady-state fluorescence to look for specific local changes around the Trp residues. Steady-state fluorescence in the presence of the acrylamide quencher revealed that the myristoylation interfered in the accessibility of some tryptophan residues (**Figure 13**B). The Stern-Volmer constant (K_{sv}) of 2.25 M^{-1} obtained for the myristoylated protein compared with K_{sv} = 3.11 M^{-1} obtained for DGRASP55 indicates that the tryptophan residues are less quenched (more protected from the acrylamide) in the myristoylated protein. This result is supported by the differences in aromatic residues environment in the near-UV CD data. It suggests changes in the microenvironment of at least one tryptophan residue of DGRASP55 after myristoylation and binding to the detergent molecules. These observations are discussed in detail in the MD simulations section below, where the surroundings of the aromatic residues in DGRASP55 and membrane-anchored myr-DGRASP55 were explored. Therefore, our near-UV and fluorescence quenching data suggest that some of the myr-DGRASP55 tryptophan residues are located in a different local environment upon myristoylation and solubilization with DDM micelles.

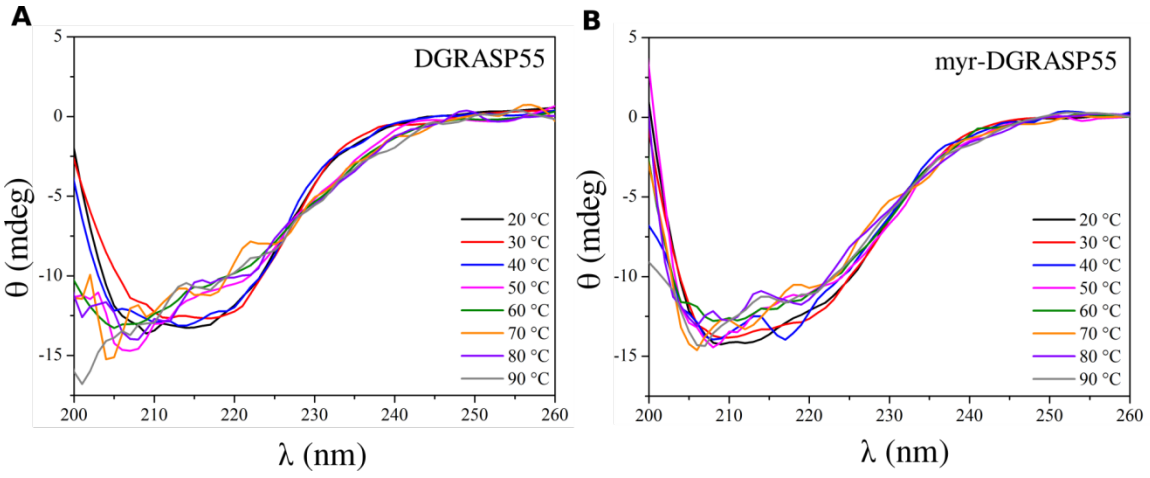

Figure 12 – (A) DGRASP55 and (B) myr-DGRASP55 far-UV spectra measured in different temperatures. Source: prepared by the author.

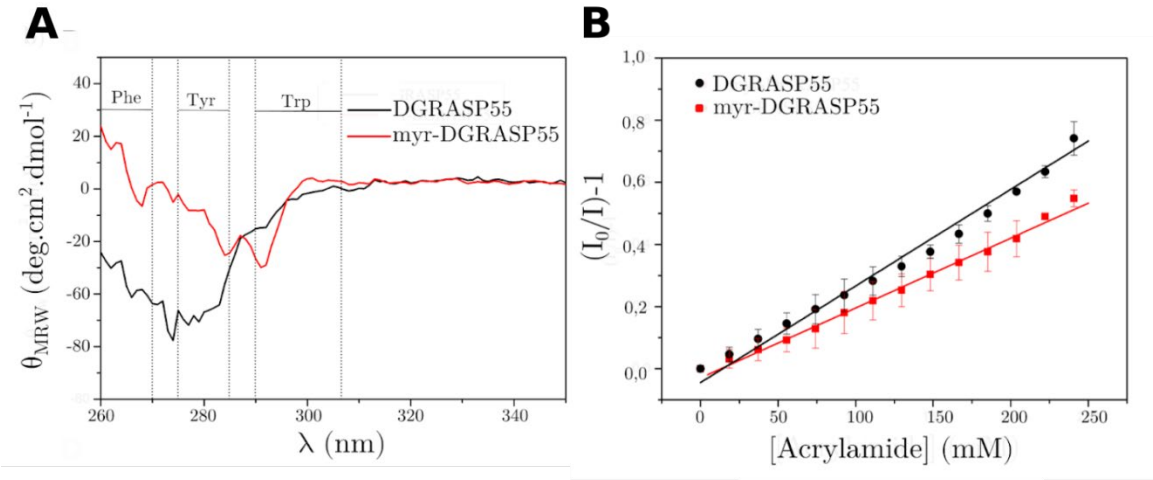

Figure 13 – (A) Near-UV spectra of DGRASP55 and myr-DGRASP55. The dashed vertical lines delimit the regions where contributions from phenylalanine, tyrosine, and tryptophan residues are expected. (B) Stern-Volmer plots showing the quenching of the tryptophan fluorescence in the presence of acrylamide. Solid lines are fits to the experimental data using the Stern-Volmer equation. Source: prepared by the author.

4.4. *Myristoylation is essential for GRASP55 membrane-anchoring*

The success of the myristoylation protocol used here was also assessed by monitoring the effective anchoring of myr-DGRASP55 in lipid membranes. The binding experiments followed the general idea published in reference 91. This was experimentally evaluated through an agarose-gel-based electrophoresis technique after incubation of liposomes with the myristoylated and the non-myristoylated protein. Overall, liposomes' electrophoresis consists of the migration of charged liposome populations of the same diameter (100 nm) in the agarose gel under a constant electric potential. This technique allowed us to study possible factors that would modify the electrophoretic mobility of liposomes, for example, alterations in the membrane charge caused by the binding of a molecule that can affect the liposome migration in the gel.

4.4.1. DMPC:POPG liposomes

In the electrophoresis assays using DMPC:POPG (4:1) lipids, a clear reduction in the electrophoretic mobility of the liposomes containing myr-DGRASP55 was observed (**Figure 14**). One interesting feature is the presence of a band at the top of the lane (indicated by a white arrow in **Figure 14**) corresponding to myr-DGRASP55-loaded liposomes that did not enter the gel. Previous data of GRASP55 tagged with a mitochondrial targeting sequence derived from the bacterial actin nucleator protein ActA of *Listeria monocytogenes* showed clustering of the mitochondria [38]. This potentially suggests that myr-DGRASP55 could induce LUV clustering by *trans*-oligomerization, which in principle increases the apparent size of the membrane structures, thus preventing them from permeating the agarose gel.

The liposomes incubated with DGRASP55 and the control sample (only liposomes in buffer solution) presented the same electrophoretic mobility of (2.59 ± 0.05) (10^{-4} cm^2 V^{-1} s^{-1}). This was significantly different from the situation observed after the incubation with myr-DGRASP55. In this case, two populations were obtained: one presenting much slower electrophoretic mobility (1.66 ± 0.05) (10^{-4} cm^2 V^{-1} s^{-1}) when compared to the control and the second population that appeared at the top of the respective lane in the gel (**Figure 14**) and could not permeate the agarose gel in the conditions tested. This indicates that myristoylation of DGRASP55 was successfully achieved, and it is essential for anchoring this protein to the membrane surface.

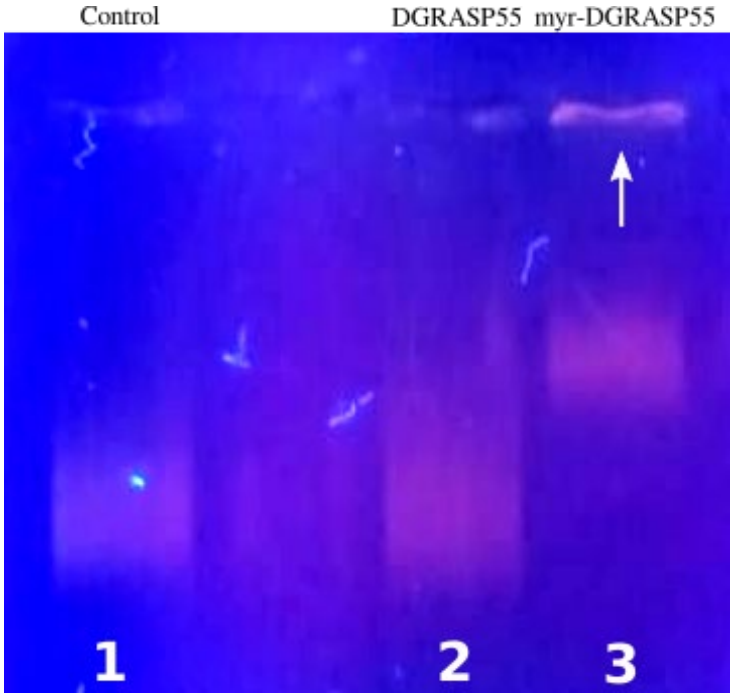

Figure 14 – Liposome electrophoretic mobility assay using DMPC:POPG (4:1) liposomes. The corresponding lanes are (1) control sample (liposomes + buffer) and samples incubated with (2) DGRASP55 and (3) myr-DGRASP55. Source: prepared by the author.

4.4.2. DMPC:DMPG liposomes

In this case, the mobility of myr-DGRASP55 incubated liposomes (DMPC:DMPG (3:2)) in the agarose gel was challenging to analyze. In the conditions tested, the liposomes incubated with the myristoylated protein did not penetrate the agarose gel (**Figure 15**). A significant quantity of liposomes was observed at the top of lane 3. This result evidenced the different mobility of pure dymiristoyl hydrocarbon chain (DMPC and DMPG) phospholipids compared to the mixed membranes composed of DMPC and POPG. The gel-to-liquid-crystalline phase transitions of these lipid hydrocarbon chains occur at temperatures around 24.1 °C (DMPC) and 23.3 °C (DMPG). They could influence the electrophoretic mobility due to the solid-like or gel phase since the LEMSA assays were not temperature-controlled. The apparent electrophoretic mobility of control and DGRASP55-loaded DMPC:DMPG liposomes was (7.42 ± 0.05) (10^{-4} cm^2 $V^{-1}s^{-1}$).

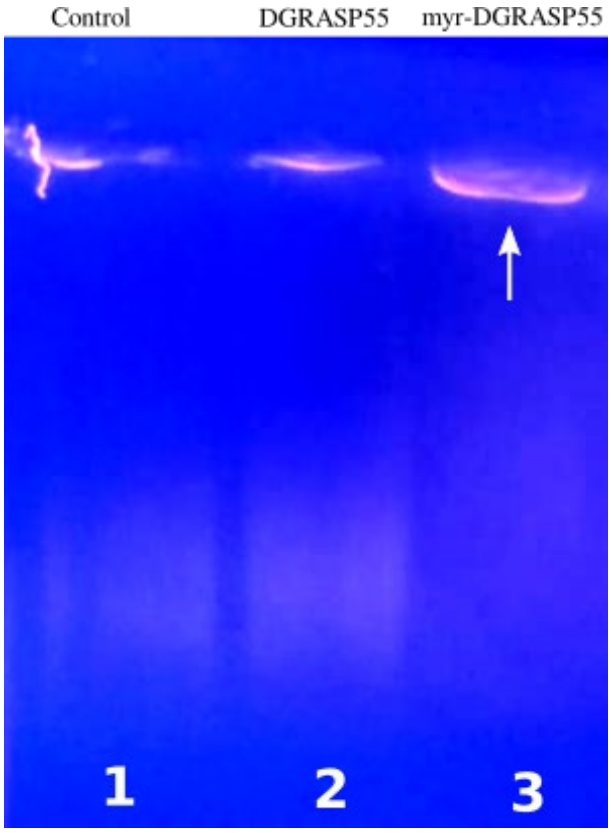

Figure 15 - Liposome electrophoretic mobility assay using DMPC:DMPG (3:2) liposomes. The corresponding lanes are (1) control sample (liposomes without protein), and samples incubated with (2) DGRASP55 and (3) myr-DGRASP55. Source: prepared by the author.

3.6.3 Heart Polar Lipid Extract (Bovine) liposomes

We also performed lipid electrophoresis assays with the natural lipids of the bovine heart (**Figure 16**). This lipid mixture is commercially available and is generally used for mimicking mammalian cellular membranes. The phospholipid profile, according to Avanti Polar Lipids, is 8.6% PC (phosphatidylcholine), 13.6% PE (phosphatidylethanolamine), 1.0% PI (phosphatidylinositol), 0.6% PA (phosphatidate), 1.7% CA (cardiolipin), 57.7% neutral lipid and 16.8% unknown. The migration behavior for this kind of liposomes, in comparison to the previous assays, had a similar pattern of lower electrophoretic mobility observed for the myr-DGRASP55-incubated lipids. The apparent electrophoretic mobility of control and DGRASP55-loaded bovine heart lipid extract liposomes was (10.73 ± 0.05) (10^{-4} cm^2 $V^{-1}s^{-1}$) and (8.48 ± 0.05) (10^{-4} cm^2 $V^{-1}s^{-1}$) for myr-DGRASP55-incubated liposomes.

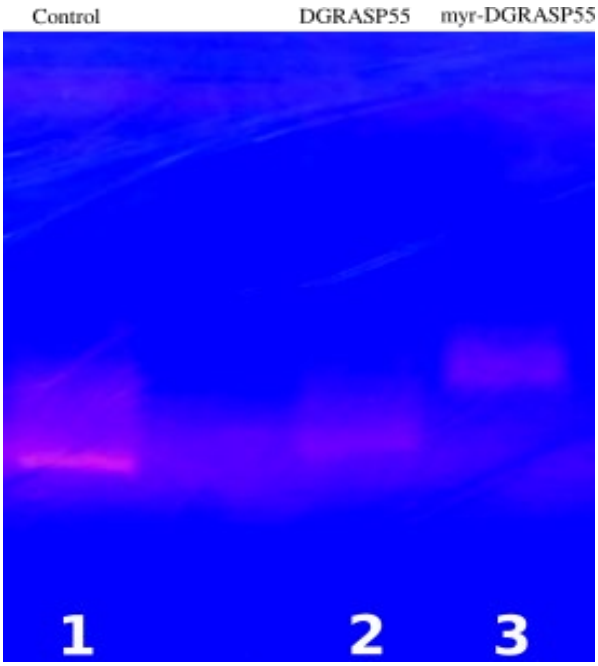

Figure 16 - Liposome electrophoretic mobility assay using Heart Polar Lipid Extract (Bovine) liposomes. The corresponding lanes are (1) control sample (liposomes without protein), and samples incubated with (2) DGRASP55 and (3) myr-DGRASP55. Source: prepared by the author.

4.5. *Exploring membrane interaction through Molecular Dynamics (MD) simulations*

To better describe the DGRASP55 membrane interaction, molecular dynamics simulations of the myristoylated and non-myristoylated proteins and a POPC model membrane were performed.

4.5.1. Initial studies

Initially, we performed three simulations (Table 1) of myr-DGRASP55 in the presence of POPC membranes with the protein in a distance that avoided any contact (distance > 3.0 Å) between the myristoyl chain and the lipid bilayer surface (**Figure 17**A-D). The minimum distances between every atom of the protein and the membrane lipids (excluding hydrogen atoms) were calculated for each simulated trajectory. The results corresponding to the first three runs are shown in **Figure 17**E. Due to the considerable distance between the protein and the membrane, runs 1 and 2 resulted in the myristate approaching the protein's C-terminal region rather than anchoring into the lipid bilayer (**Figure 17**B-C). On the other hand, in run 3, the myristate entered into the protein core and did not stay close to the C-terminal region as in runs 1 and 2 (**Figure 17**D). Thus, these first runs showed that the localization of the myristoyl chain close to the protein's C-terminus (runs 1 and 2) led to the closest approximation to the membrane.

Table 1 – Summary of MD simulations performed in the first attempts of a myr-DGRASP55 and POPC model membrane. Source: prepared by the author.

Run	Time (ns)	Protein	Result
1	550	myr-DGRASP55	The myristoyl chain stayed close to the C-terminal region.
2	550	myr-DGRASP55	Protein kept the lowest average protein-membrane minimum distance compared to runs 1 and 3 and myristate approaches to the C-terminal region.
3	550	myr-DGRASP55	Protein kept a greater distance than the observed in runs 1 and 2. The myristoyl got inside the protein core.

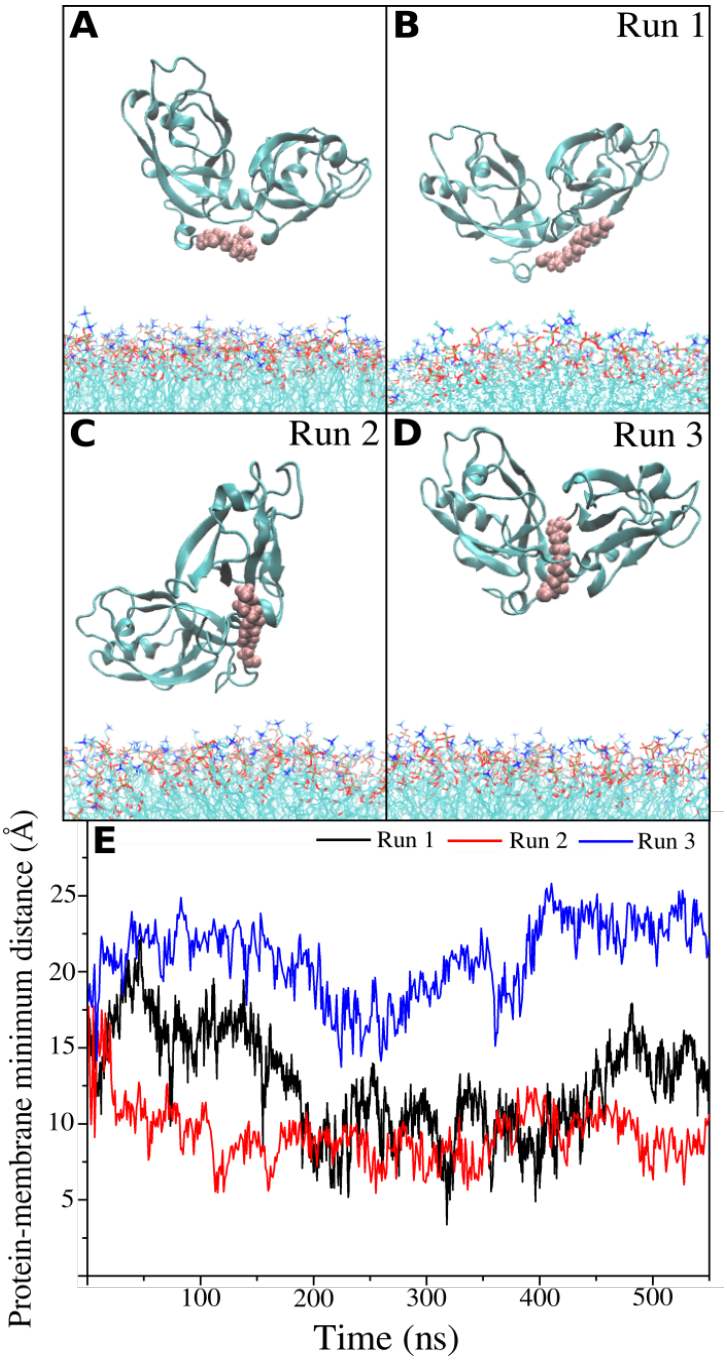

Figure 17 – First simulations of myr-DGRASP55 and POPC lipid bilayer. Simulations started with the exposed myristoyl chain as represented in (A) and after 550 ns resulted in the explicit approximation between the C-terminal region and the myristate represented in (B) run 1 and (C) run 2. The result of run 3 is represented in (D). Minimum distances between protein and POPC atoms in all three runs are shown in (E). Source: prepared by the author.

4.5.2. Removing the myr-DGRASP55 C-terminal region

The results of the first attempts presented in the previous section led us to keep a similar initial configuration with the POPC membrane, but now removing part of the C-terminal residues, hence trying to avoid the effects previously observed in runs 1 and 2. Then, we performed more simulations to check whether the protein would get closer or eventually anchor into the bilayer. Two runs of these simulations (Table 2) resulted in the myristate entering into the protein core (**Figure 18**), a similar result to the one observed in run 3.

Table 2 – Summary of the simulations of myr-DGRASP55 performed without the C-terminal residues (197-207) and a POPC model membrane. Source: prepared by the author.

Run	Time (ns)	Protein	Result
4	150	myr-DGRASP55	Myristate entered into the protein core in less than 10 ns.
5	150	myr-DGRASP55	Similar to run 4, the myristate entered into the protein core in less than 10 ns.

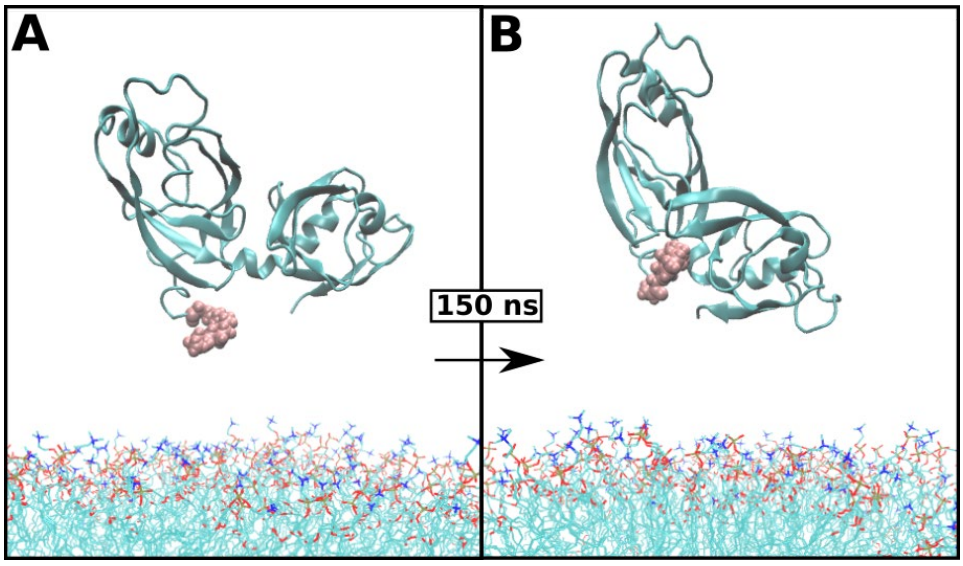

Figure 18 – Simulation of myr-DGRASP55 (run 4) without the C-terminal region (residues 197-207) started in the configuration represented in (A) and resulted in the entrance of the myristate into the protein core (B). Source: prepared by the author.

4.5.3. Decreasing protein-membrane distance

The unsuccessful docking of the DGRASP55 to the membrane described in the subsections above made us change the protein orientation relative to the membrane surface. Previously, Heinrich *et al*. (2014) [75] reported neutron scattering data on the orientation of DGRASP55 in a membrane model system. In that case, the anchoring to the membrane was achieved using both the Gly2 myristoylation and the interaction of a 6-His-tag located in the C-terminus of DGRASP55 with a 1,2-dioleoyl-sn-glycero-3-[(N-(5-amino-1-carboxypentyl)iminodiacetic acid)succinyl] phospholipid inserted in the model membrane. Therefore, our simulations of the DGRASP55 started with the protein in an orientation relative to the membrane as described by Heinrich *et al*. (2014) [75] (**Figure 19**A). Moreover, the simulations of myr-DGRASP55 started in a configuration where the myristoyl chain was partially inserted into the bilayer (**Figure 19**B), resulting in the restriction of the protein to a position close to the membrane, which was maintained along all calculated trajectories (**Figure 19**C). The summary of this round of simulations is seen in **Table** 3.

Table 3 – Summary of the simulations of DGRASP55 and myr-DGRASP55 performed with a closer initial distance between protein and membrane and different orientations in relation to the first attempts shown in the previous subsections. Source: prepared by the author.

Run	Time (ns)	Lipids	Protein	Result
6	780	POPC	myr-DGRASP55	Myristate penetrated deeper into the bilayer in an effective anchoring, and the protein-membrane minimum distance was stabilized
7	515			
8	580	POPC:POPG (4:1)		
9	580			

10	1570	POPC	DGRASP55	Protein moved away from the membrane in approximately 800 ns.
11	500			The protein stayed in a similar minimum distance as in the first frame. However, the time of simulation was not enough to observe any protein detachment.

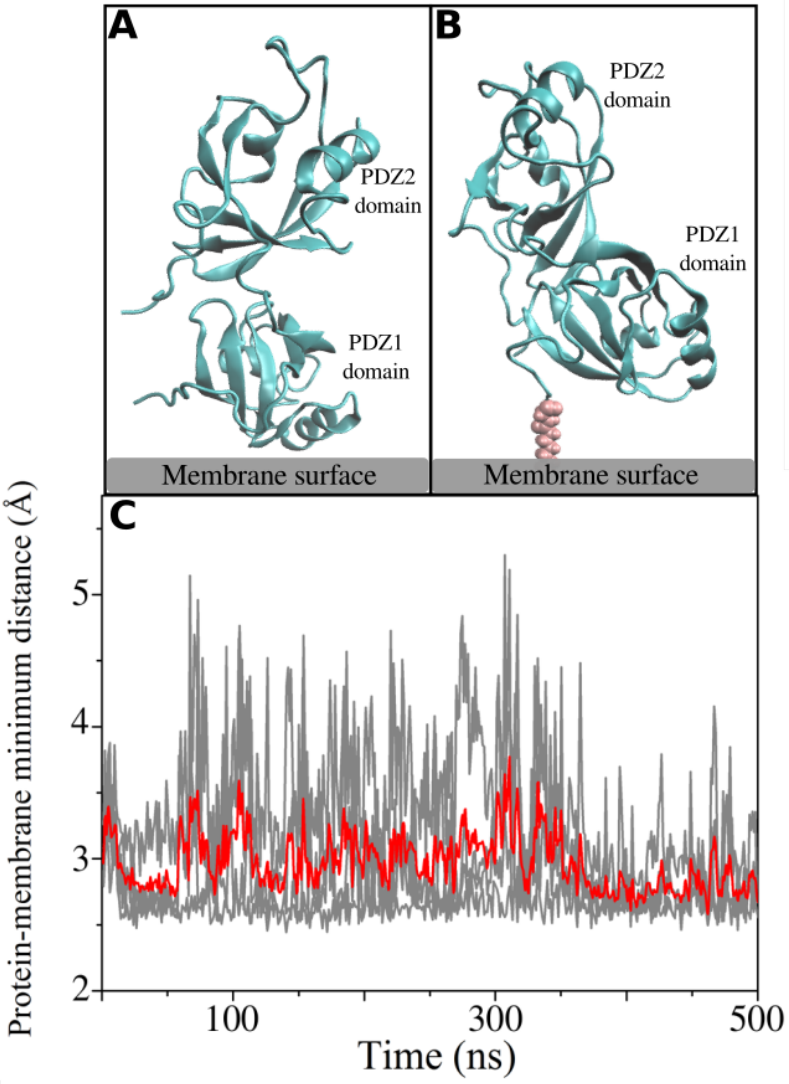

Figure 19 – (A) DGRASP55 orientation relative to the membrane surface described by Heinrich *et al*. (2014) [75]. (B) myr-DGRASP55 initial orientation used in our simulations. (C) Minimum distance between the atoms of anchored myr-DGRASP55 and the lipid residues in four different trajectories. The myristoyl chain penetrated slightly more into the bilayer in all trajectories, and the minimum distance was stabilized. The gray lines represent the data calculated for each

trajectory, and the red line is the average minimum distance between simulations. Source: prepared by the author.

In those rounds of simulations (runs 10 and 11) of the DGRASP55, we observed the protein detaching from the membrane (**Figures 20**A-B) in a short timescale of approximately 800 ns, thus highlighting the instability of any interaction between the non-myristoylated protein and the lipid membranes. This agrees with our experimental results in subsection 4.4. In the simulations of myr-DGRASP55 (**Figure 20**C), the membrane anchoring was achieved without the need for the artificial 6-His-tag anchoring strategy used by Heinrich *et al.* (2014), which likely resulted in a tilted orientation towards the membrane surface in our model (**Figure 21**) when compared to that obtained by those authors [75]. As a result, some of the aromatic residues of myr-DGRASP55 (highlighted in colors in **Figure 20**B) were less accessible to the solvent, as we show in the surface-accessible surface area (SASA) data (**Figures 22-26**). As said above, we did not observe the detachment of the protein due to the myristoyl-anchoring, which kept those aromatic residues (Tyr16, Tyr165, and Phe206) more or less accessible to the solvent. Moreover, we observed a series of residues that were in constant contact (distance < 3.0 Å) with the phospholipids along the simulated trajectories. The residues in contact with the bilayer belong to the following regions: residues 43 to 45 (Asn43, Gly44, and Ser45), 60 to 67 (Ala60, Asn61, Val62, Glu63, Lys64, Pro65, Val66, and Lys67), and 80 to 82 (Glu80 and Ser82) (**Figure 27**).

The occupancy of the contacts calculated for each region (**Figure 27**A) in the two trajectories of myr-DGRASP55 are shown in **Table 4**. We examined the salt bridges formed between residues in contact with the lipids and observed a greater involvement of basic residues (Lys64 and Lys67) in the protein-membrane interfacial region (**Figure 28**). This result suggests a possible role for the electrostatic interactions, between these regions of the protein (**Figure 27**B) and the charged membrane surface. We have also calculated the number and hydrogen bonds between lipids and proteins along the trajectories summarized in **Table 3**, as we show in **Figure 29**. The presence of this network of interactions is important because it was shown before that the binding energy provided by the myristoylation only is weak (K_D of ~10^{-4} M), and hence insufficient to

fully anchor a protein to the membrane [92]. Our MD data suggest that a coupled mechanism, which includes the Gly2 myristoylation and a series of interactions between amino acids of myr-DGRASP55 with the membrane surface, is responsible for the restricted configuration of GRASP55 in membranes, necessary to avoid the cis-oligomerization.

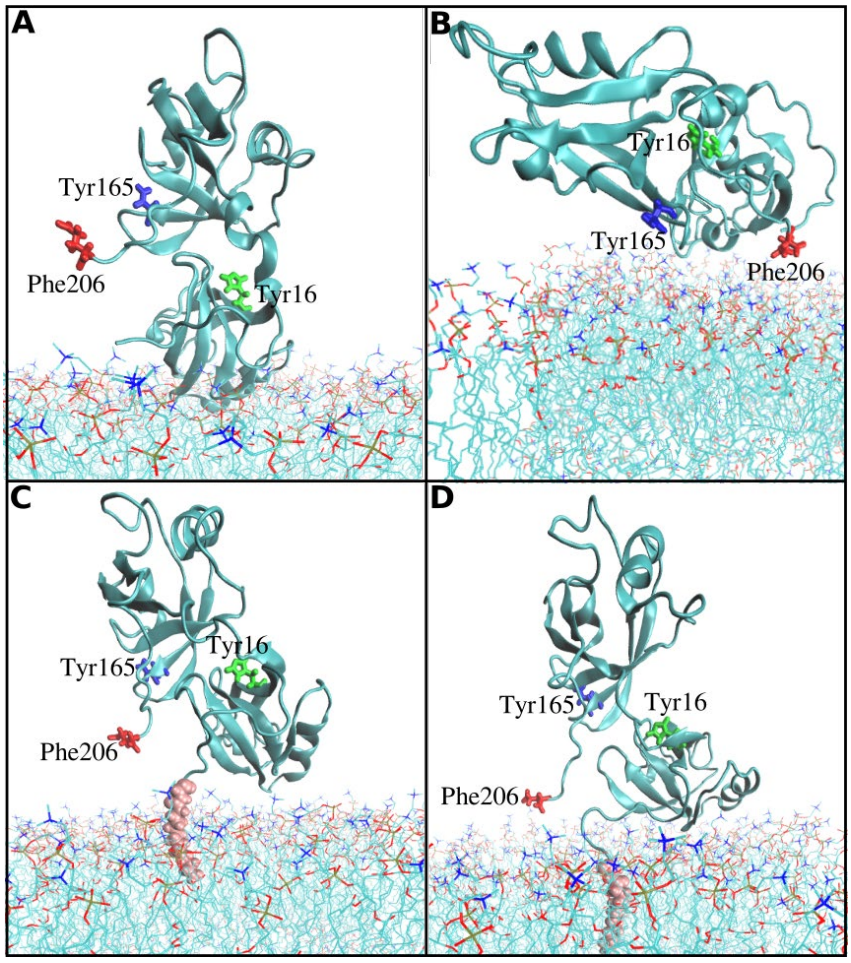

Figure 20 – MD simulations of DGRASP55 and myr-DGRASP55 in contact with a model membrane. Mobility of DGRASP55, starting from the orientation represented in (A) and resulting in the detachment from the membrane surface observed in (B) after 1.4 μs. Simulations of the myr-anchored protein started with the orientation represented in (C) and resulting in the orientation shown in (D) after 780 ns. The aromatic residues are shown in licorice representation: Tyr16 (green), Tyr165 (blue) and Phe206 (red). Pink spheres represent the myristoyl group. Lipids in the membrane are shown as lines, hydrocarbon chains are colored in cyan, and headgroups are colored in red (oxygen), ocher (phosphorus), and blue (nitrogen). Source: prepared by the author.

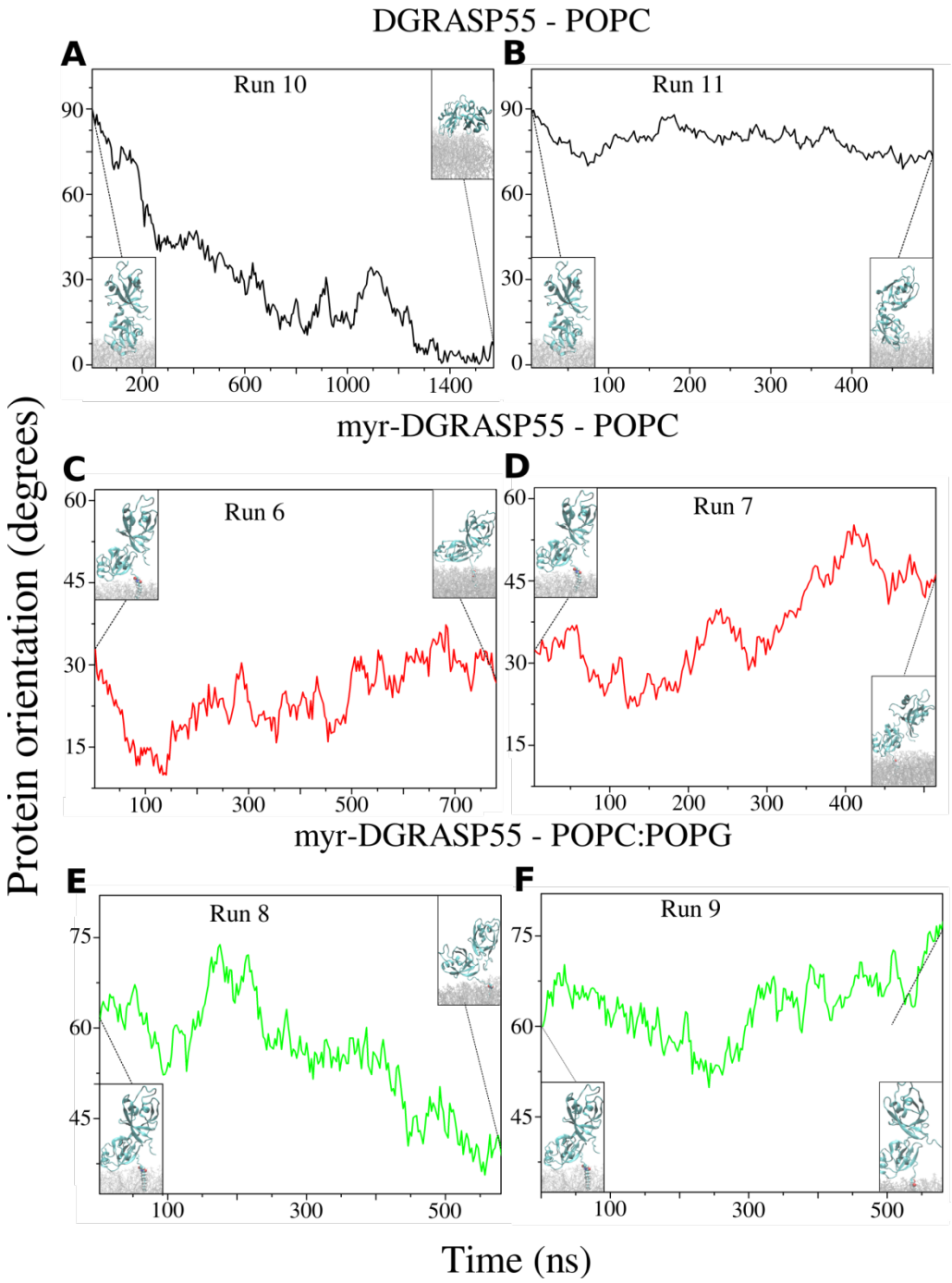

Figure 21 - Protein orientation relative to the membrane surface calculated for six different trajectories. The images on the graph's left side represent the protein orientation at the first frame, and images on the right side represent the last simulation frame. The angle formed between the POPC bilayer surface and a principal axis passing through the protein center of mass is shown for A, B) DGRASP55 and C, D) myr-DGRASP55. The orientation of myr-DGRASP55 relative to a POPC:POPG (4:1) bilayer calculated for two trajectories is shown in E) and F). Source: prepared by the author.

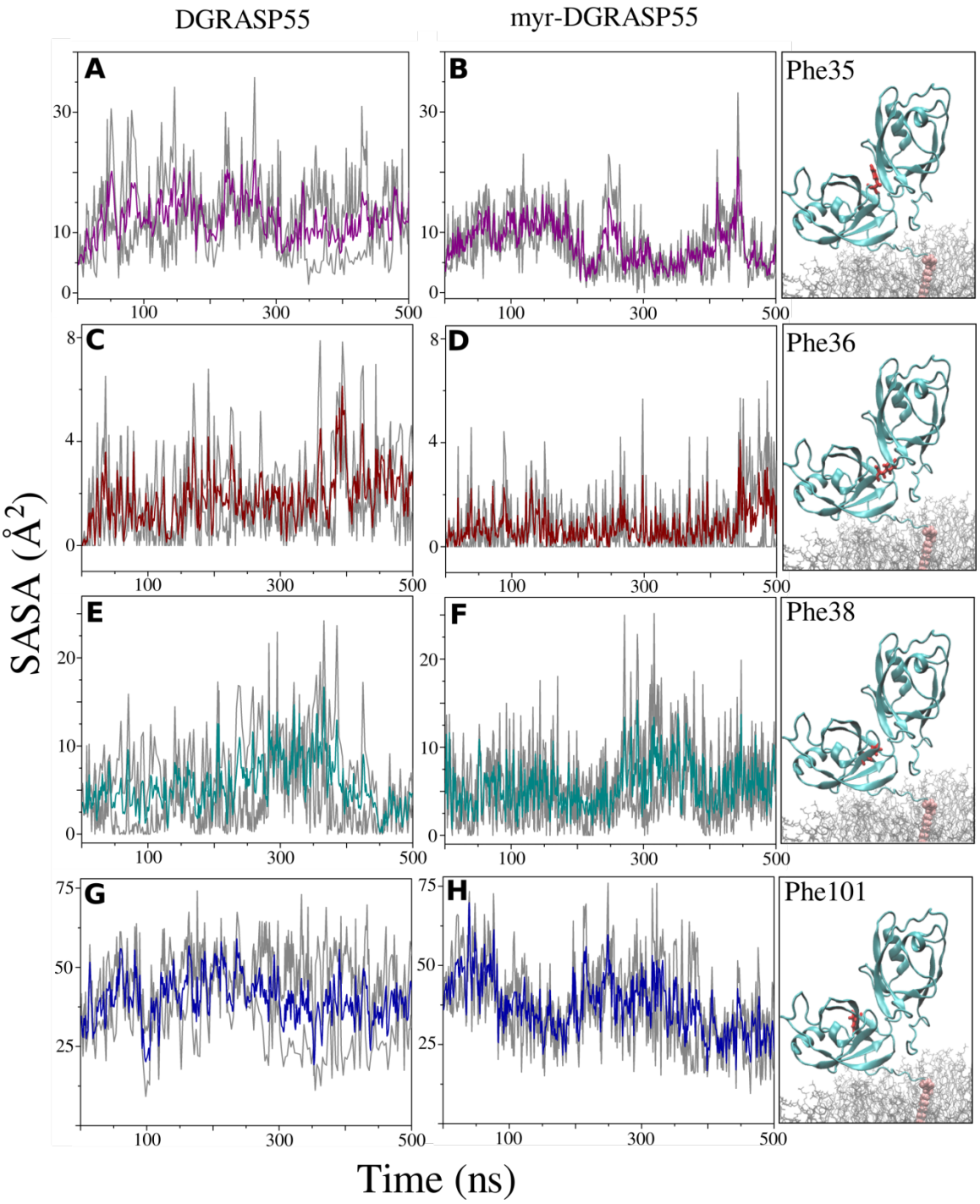

Figure 22 - Solvent accessible surface area (SASA) calculated for phenylalanine residues in the simulations with a POPC membrane. The images at the right side represent the location of the residue (colored in red) in the myristoyl-anchored protein. The SASA data of Phe35, Phe36, Phe38 and Phe101 residues are calculated for A, C, E, G) DGRASP55 and B, D, F, H) myr-DGRASP55. The lines in gray represent the SASA of each individual trajectory, and the colored lines represent the average between runs 6 and 7. Source: prepared by the author.

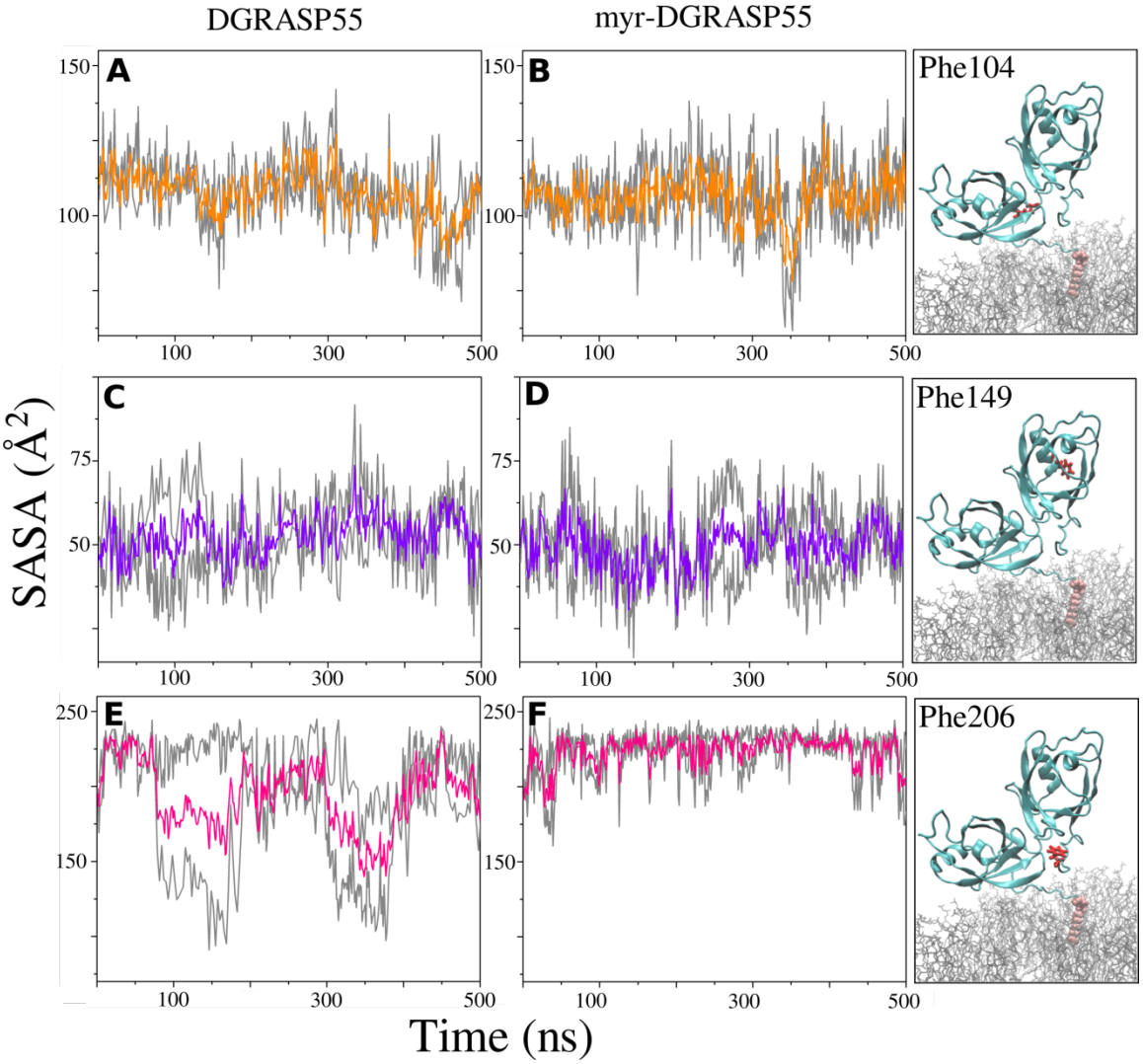

Figure 23 - Solvent accessible surface area (SASA) calculated for phenylalanine residues in the simulations with a POPC membrane. The images at the right side represent the location of the residue (colored in red) in the myristoyl-anchored protein. The SASA data of Phe104, Phe149 and Phe206 residues are calculated for A, C, E) DGRASP55 and B, D, F) myr-DGRASP55. The lines in gray represent the SASA of each individual trajectory, and the colored lines represent the average between runs 6 and 7. Source: prepared by the author.

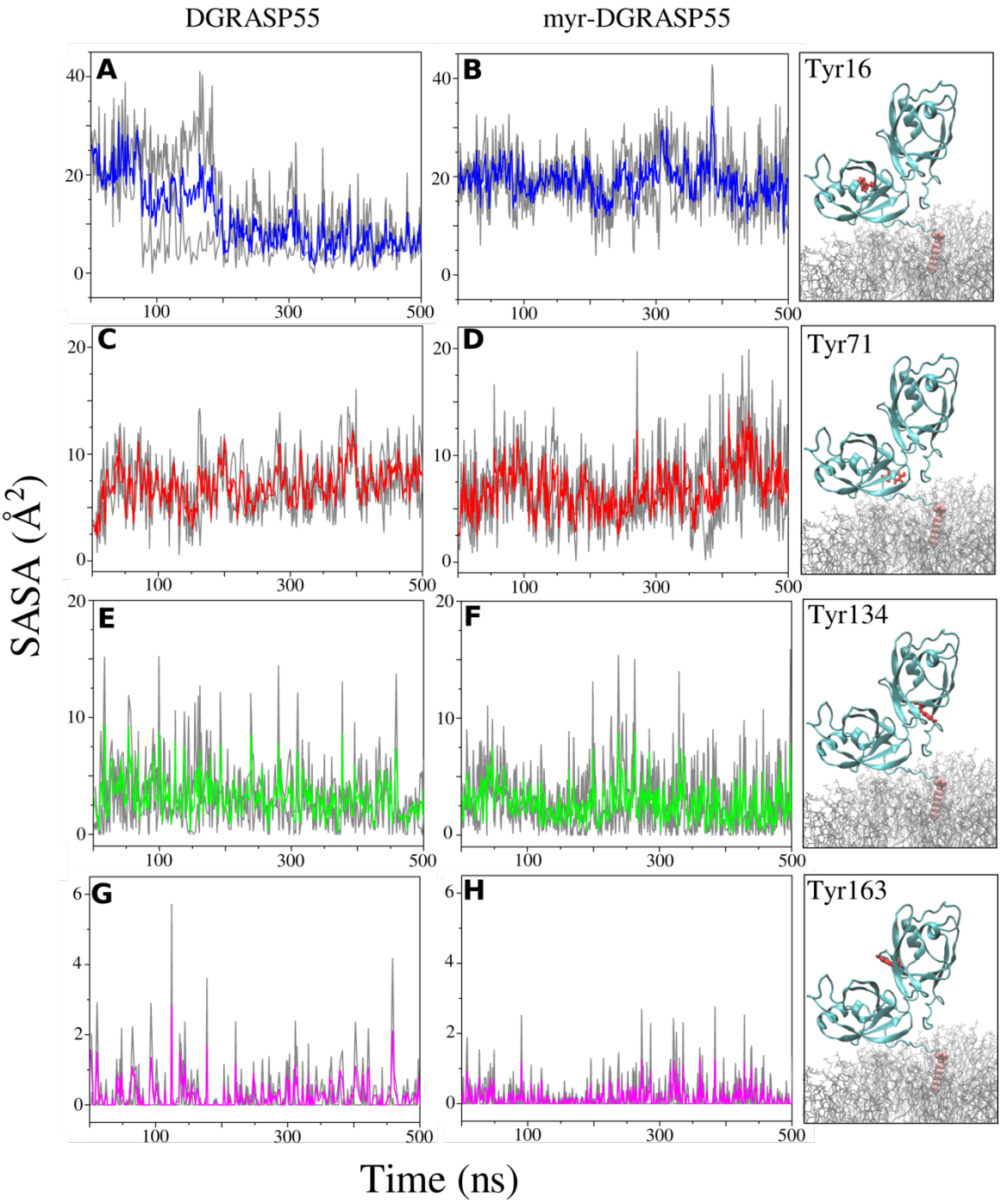

Figure 24 - Solvent accessible surface area (SASA) calculated for tyrosine residues in the simulations with a POPC membrane. The images at the right side represent the location of the residue (colored in red) in the myristoyl-anchored protein. The SASA data of Tyr16, Tyr71, Tyr134 and Tyr163 residues are calculated for A, C, E, G) DGRASP55 and B, D, F, H) myr-DGRASP55. The lines in gray represent the SASA of each individual trajectory, and the colored lines represent the average between runs 6 and 7. Source: prepared by the author.

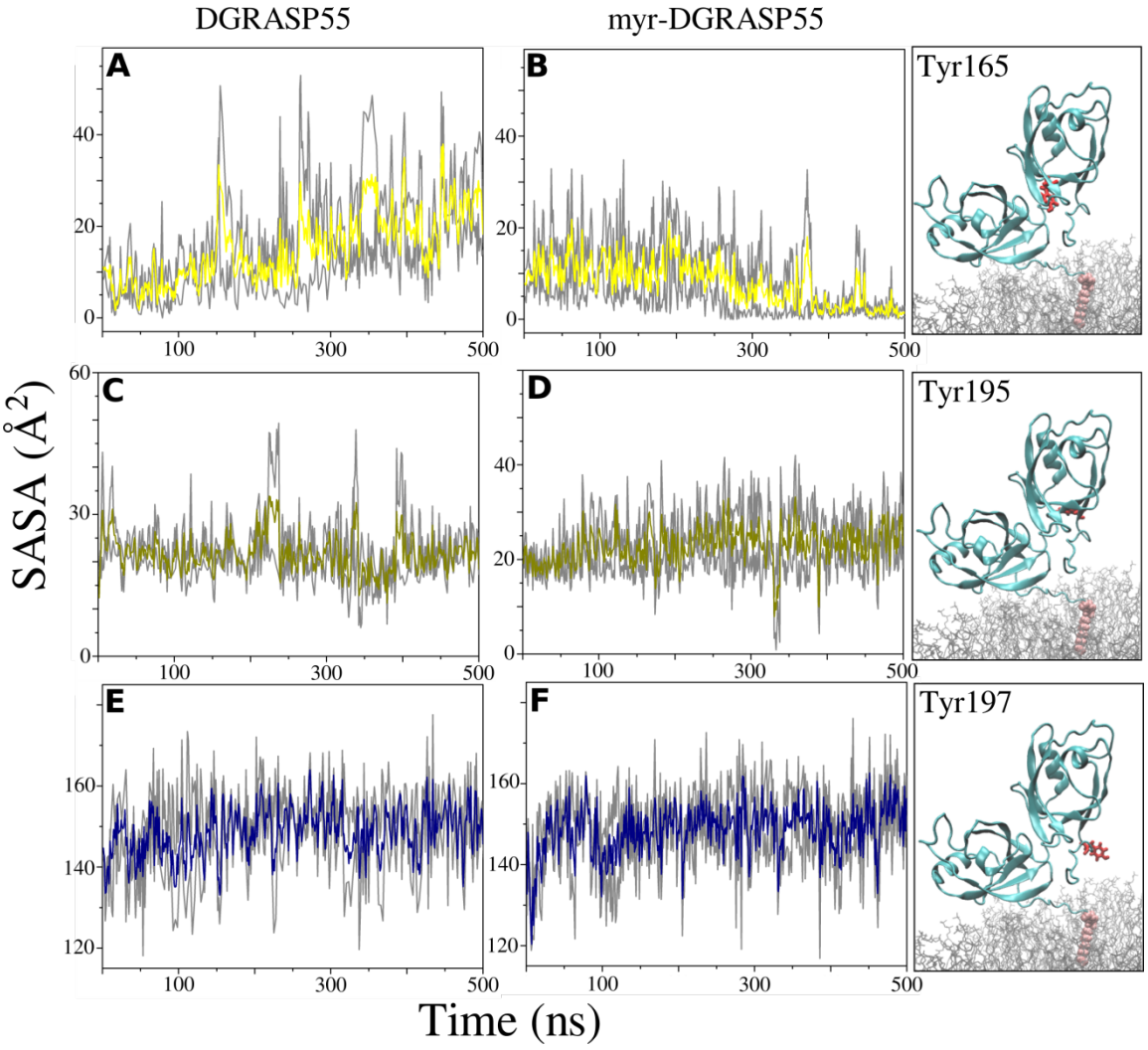

Figure 25 - Solvent accessible surface area (SASA) calculated for tyrosine residues in the simulations with a POPC membrane. The images at the right side represent the location of the residue (colored in red) in the myristoyl-anchored protein. The SASA data of Tyr165, Tyr195, and Tyr197 residues are calculated for A, C, E) DGRASP55 and B, D, F) myr-DGRASP55. The lines in gray represent the SASA of each individual trajectory, and the colored lines represent the average between runs 6 and 7. Source: prepared by the author.

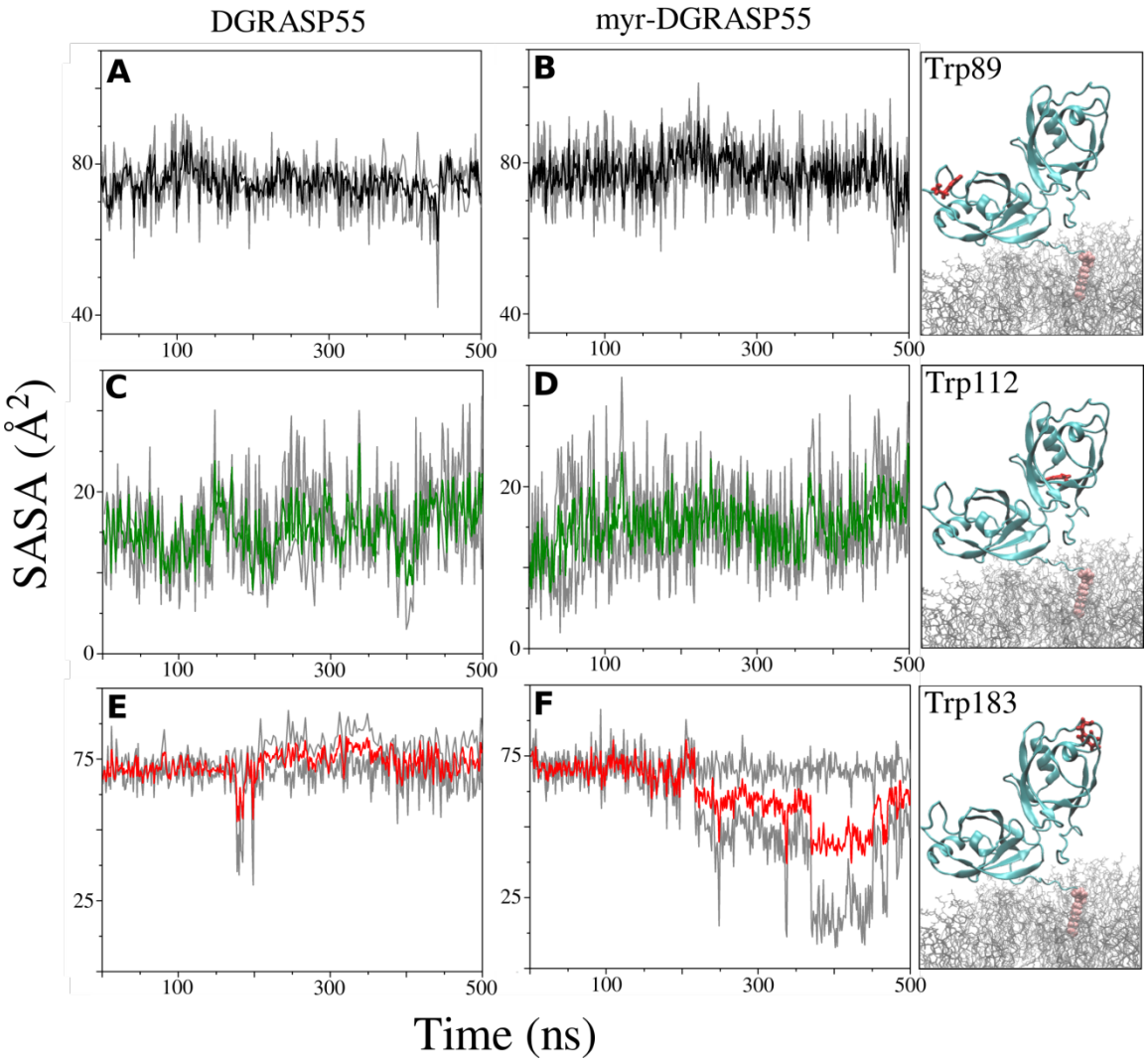

Figure 26 - Solvent accessible surface area (SASA) calculated for tryptophan residues in the simulations with a POPC membrane. The images at the right side represent the location of the residue (colored in red) in the myristoyl-anchored protein. The SASA data of Trp89, Trp112, and Trp183 residues are calculated for A, C, E) DGRASP55 and B, D, F) myr-DGRASP55. The lines in gray represent the SASA of each individual trajectory, and the colored lines represent the average between runs 6 and 7. Source: prepared by the author.

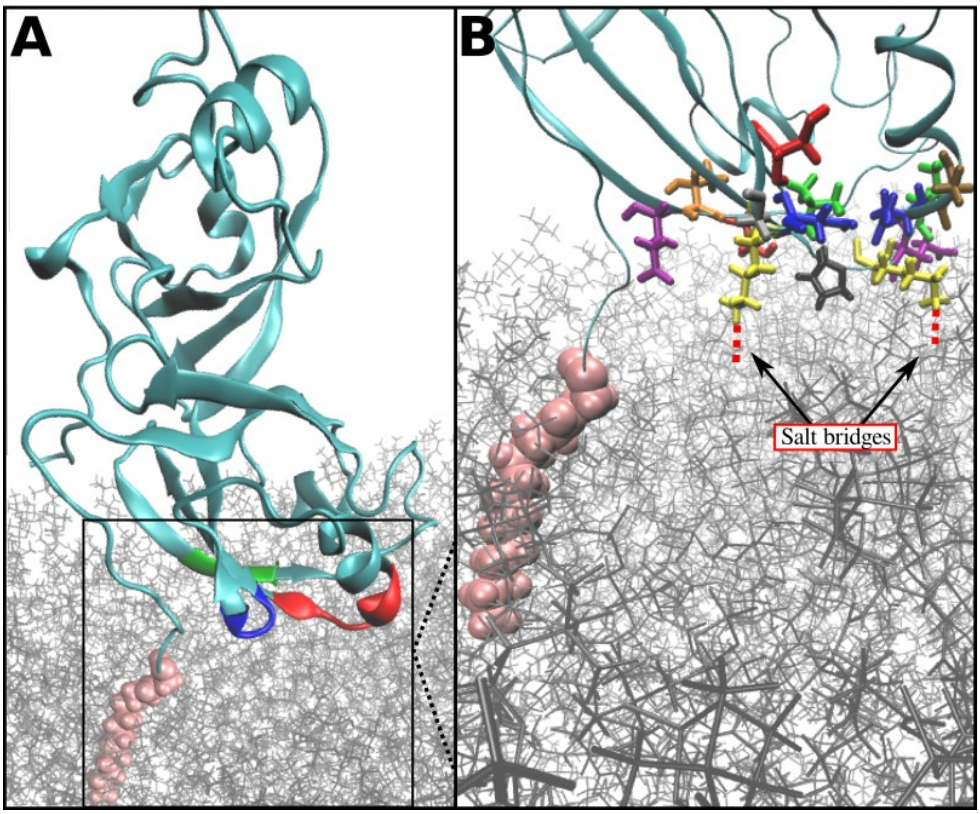

Figure 27 – (A) Regions at the protein-membrane interface in contact with the lipid bilayer. The regions are colored in blue (residues 43 to 45), red (residues 60 to 67), and green (80 to 82). (B) Details of the interfacial region identifying specific amino acid residues, drawn as licorice representation and colored in blue (Asn43 and Asn61), red (Ser45 and Ser82), yellow (Lys64 and Lys67), gray (Gly44), green (Val62 and Val67), orange (Thr81), purple (Glu63 and Glu80), ocher (Ala60) and black (Pro65). The red dashed lines indicate the salt bridges formed between lipids and protein. Lipids are represented as gray sticks, and myristate is represented as pink spheres. Source: prepared by the author.

Table 4 - Residue occupancy calculated for each residue in contact (distance < 3.0 Å) with the lipid bilayer in each simulation. The occupancy is defined as the fraction of simulation time in which the residue is in contact with lipids. Source: prepared by the author.

Protein	**DGRASP55**		**myr-DGRASP55**			
Simulation	10	11	6	7	8	9
Residue	**Occupancy (%)**					
Gly1	0,18	0,74	47,85	38,17	42,41	36,98
Ser2	0	0	4,30	32,79	64,05	47,11
Ser3	0	3,97	4,01	18,73	8,06	45,87
Gln4	7,88	2,48	1,00	13,11	2,89	13,02
Ser5	0	0,74	0	0,23	0,41	0
Val6	2,15	0,50	0	0	0,21	0
Glu7	5,38	14,39	0	0	1,03	0,21
Ile8	1,07	0,99	0	0	0,83	0

Pro9	1,07	0,25	0	0	0	0
Gly10	0,90	12,16	0	0	0	0
Asn24	3,05	0	0	0	0	0
Arg29	1,43	1,98	0	0	0	0
Ser41	3,22	0,25	0	0	0	0
Ile42	0,54	2,98	0	0	0	0
Asn43	1,79	44,91	0	2,34	0,83	2,48
Gly44	3,94	44,17	0	1,87	0,62	1,24
Ser45	1,97	37,96	0	0,70	0	0,21
Arg46	0,36	26,30	0	0	0	0
Arg48	0,36	0,25	0	0	0	0
Lys49	1,44	15,88	0	0	0	0

Asn51	4,84	5,46	0	0	0	0
Asp52	2,51	2,48	0	0	0	0
Thr53	4,84	4,22	0	0	0	0
Lys55	0	59,06	0	0	0	0
Asp56	1,43	3,47	0	0	0	0
Lys59	1,61	92,30	0	0	0	0
Ala60	1,07	3,72	0	1,87	0	3,72
Asn61	12,36	41,44	0	3,04	0	0,62
Val62	0	0,49	0	0,93	0	0,62
Glu63	1,075	18,61	0,18	8,90	0,83	6,45
Lys64	22,58	49,63	0	51,05	5,99	35,12
Pro65	0,72	0,25	0,18	2,11	0	2,45
Val66	2,15	0	0	0	0	0

Lys67	6,09	31,76	0	26,46	2,45	26,24
Glu77	0	0	0	0	0,21	0,21
Glu80	0	1,16	1,43	3,51	0,83	2,69
Thr81	0,36	0	0	0	0	0
Ser82	0	2,73	0,18	2,58	0	0,62
Ser83	2,87	0	0	0	0	0
Thr84	1,07	20,35	0	0	0,21	0
Asn87	0	21,83	0	0	0	0
Leu88	1,43	6,95	0	0	0	0
Trp89	0	0,99	0	0	0	0
Gly90	2,33	2,48	0	0	0	0
Gly91	0,18	5,46	0	0	0	0
Gln92	3,58	7,19	0	0	0	0

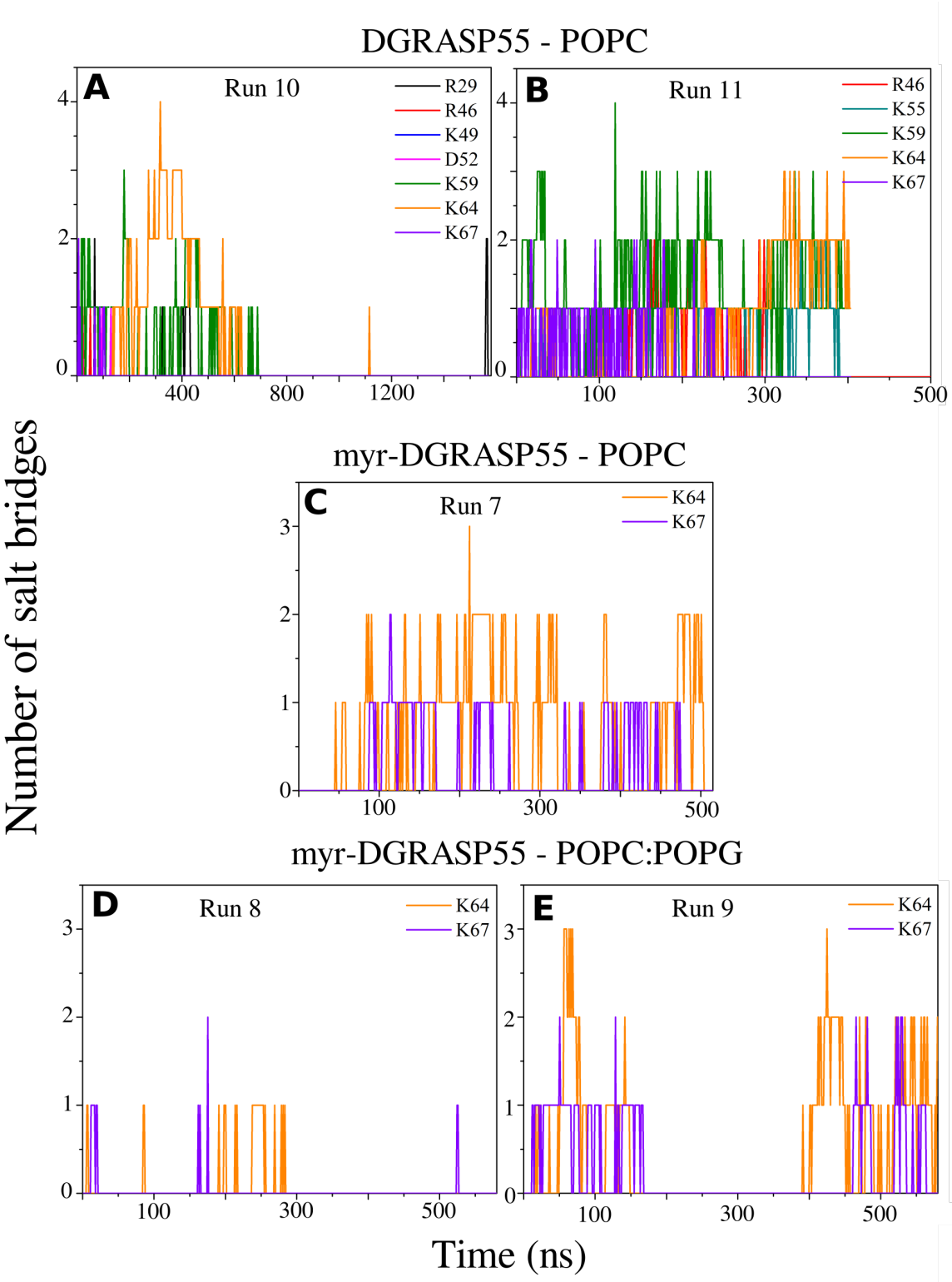

Figure 28 – Salt bridges formed between protein and lipids along five trajectories. The residues involved in these salt bridges are shown by different colors. The number of salt bridges formed is shown for A, B) DGRASP55 and a POPC bilayer, C) myr-DGRASP55 and POPC bilayer and D, E) myr-DGRASP55 and a POPC:POPG (4:1) bilayer. There were no salt bridges between lipids and protein in the simulation 1 of myr-DGRASP55 and POPC membrane. Source: prepared by the author.

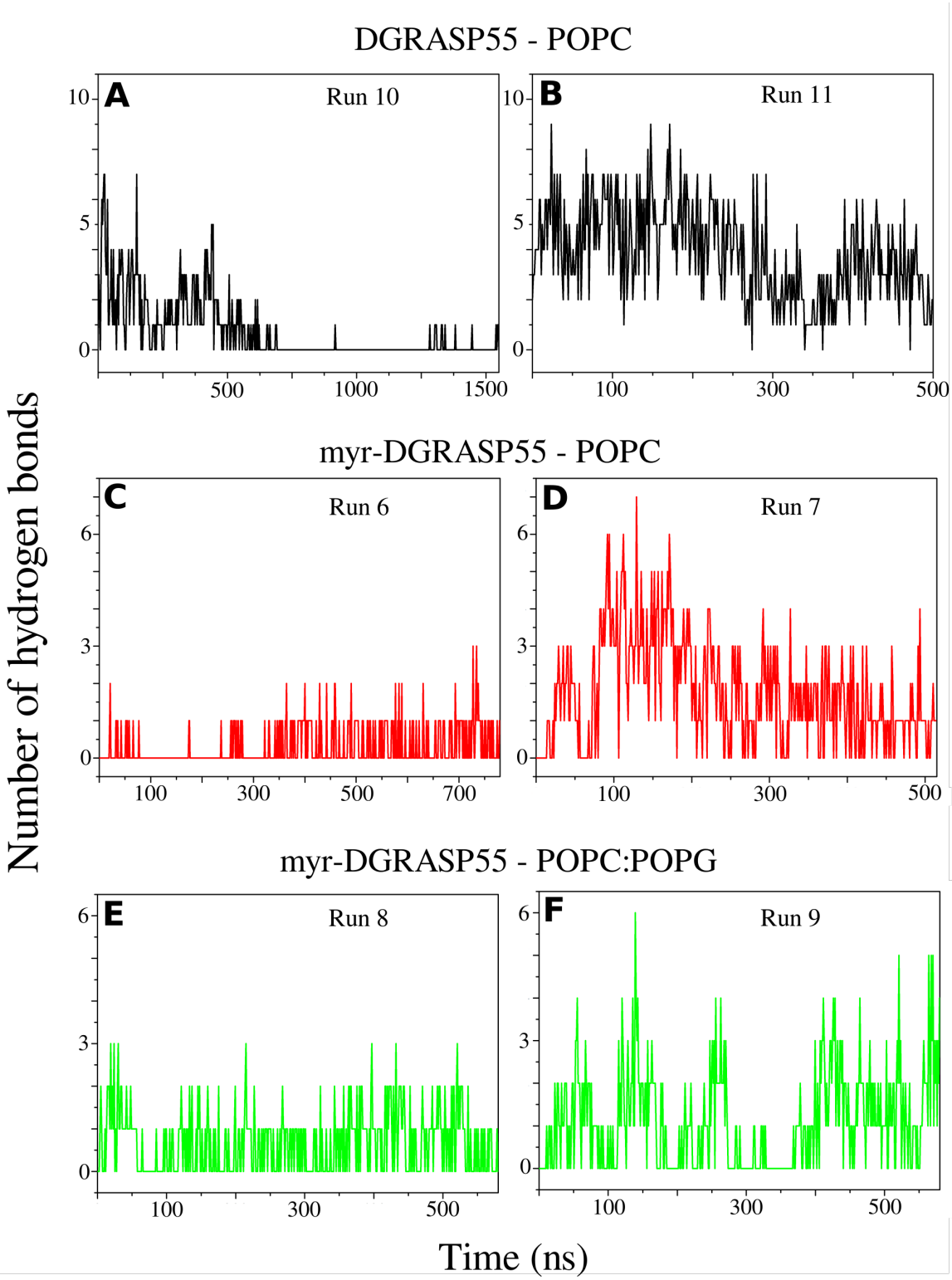

Figure 29 - Hydrogen bonds formed between protein and lipids along six trajectories. The number of hydrogen bonds formed is shown for A, B) DGRASP55 and a POPC bilayer, C, D) myr-DGRASP55 and POPC bilayer and E, F) myr-DGRASP55 and a POPC:POPG (4:1) bilayer.

4.5.4. New orientation for DGRASP55 in the membrane

From the results discussed in the previous section, we were able to see that the PDZ1 domain (residues 15 to 105) had an essential role in binding at the membrane surface. Since in the simulations described in subsection 4.5.3 we started the simulations in a configuration with the PDZ1 faced to the membrane, we decided to check the protein behavior changing to a configuration where the two PDZs lay parallel to the bilayer surface. MD simulations were performed with DGRASP55 in an initial orientation, as shown in **Figure 30**A. In run 12 (**Figure 30**B), the protein surprisingly rotated its PDZ1 towards the lipid bilayer, assuming an orientation similar to the one used as a starting configuration in the simulations of section 4.5.3. Run 13 resulted in the detachment of the protein from the membrane (**Figure 30**C). At the end of run 14 (**Figure 30**D), DGRASP55 kept the parallel orientation towards the membrane surface. Run 15 also resulted in a protein approximation to the membrane surface with the PDZ1 remaining close to the bilayer (**Figure 30**E). The minimum distances between protein and membrane atoms calculated for all four simulations are represented in **Figure 30**F.

Table 5 – Summary of the simulations of DGRASP55 performed with the protein in a parallel orientation to the POPC membrane surface. Source: prepared by the author.

Run	Time (ns)	Result
12	1334	Around 240 ns, the protein rotated from the first parallel orientation and approximated the membrane surface.
13	555	Protein moved away from its first distance relative to the bilayer.
14	1255	Protein approximated the membrane without changing its orientation.
15	635	Protein approximated the membrane, slightly changing its orientation relative to the first position.

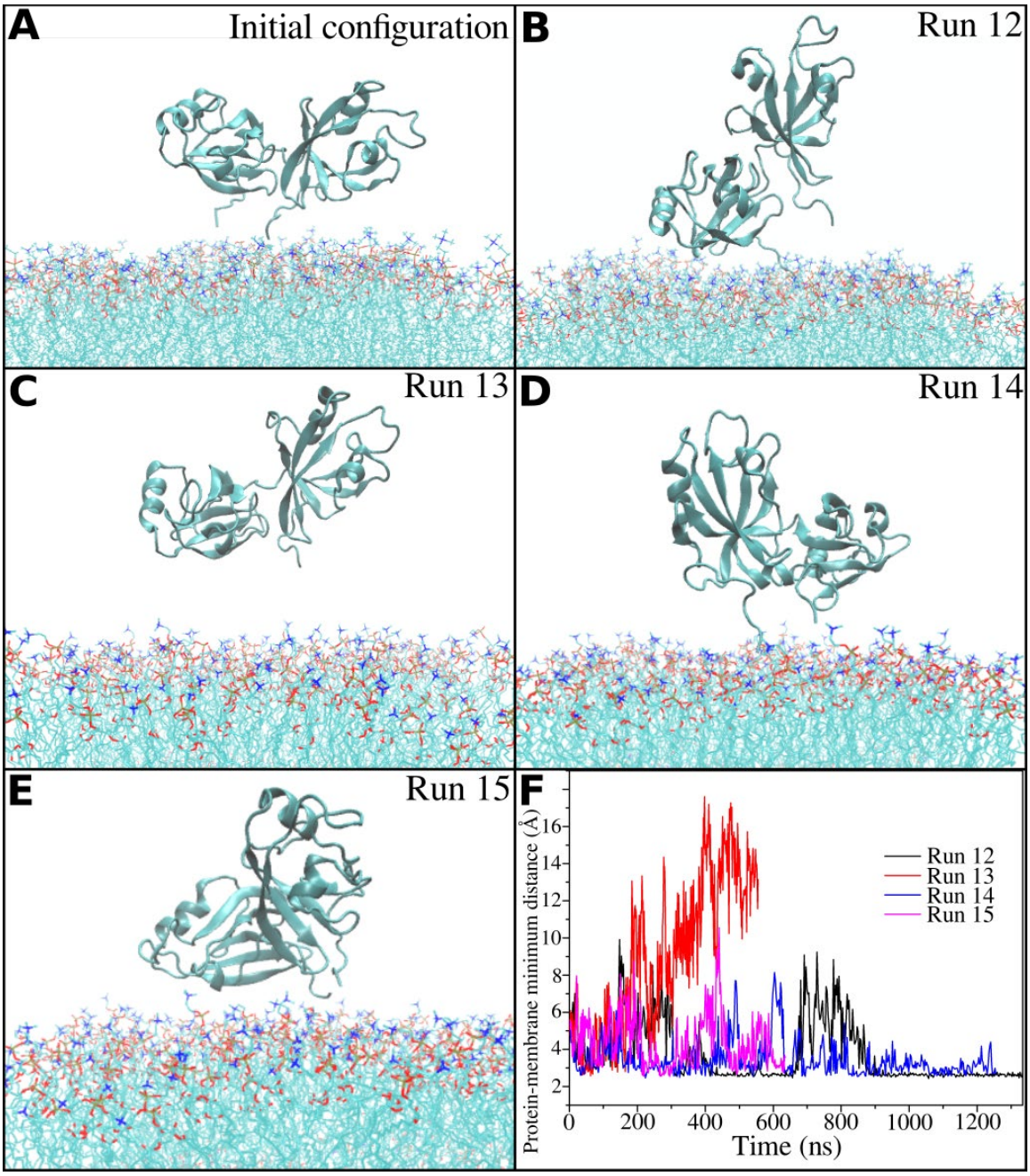

Figure 30 - Results of MD simulations showing DGRASP55 and the membrane in four different ways. The simulations started from the same configuration represented in (A). The final trajectory frame of run 12 is illustrated in (B), run 13 in (C), run 14 in (D), run 15 in (E). The minimum distances between protein and membrane calculated for each trajectory are shown in (F). Source: prepared by the author.

Figure 31 shows the number of contacts between the protein and the membrane in the two most extended simulations. There was an increase in the average number of contacts for run 12 compared with run 14. This increase in protein-membrane contacts in simulation 12 indicates that DGRASP55 has a tilted preferential orientation to the lipid membrane, where the PDZ1 domain kept closer to the bilayer surface.

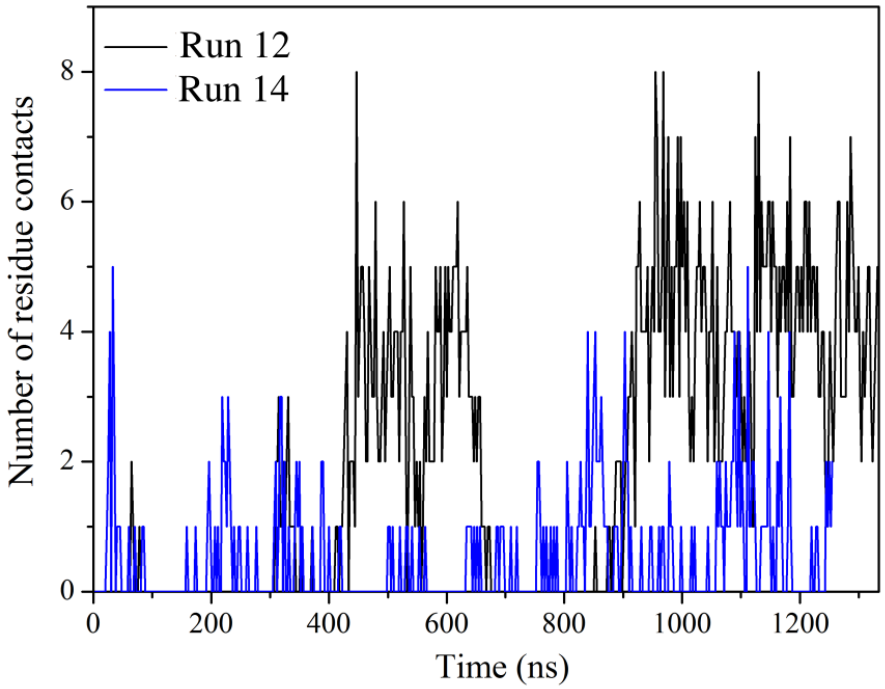

Figure 31 – Number of contacts calculated for the two most extended simulated trajectories shown in **Figure 30**B and **Figure 30**D. The final orientation in run 12 allows more protein-membrane contacts with the bilayer, suggesting a preference for a PDZ1-membrane interface in an orientation similar to the one adopted by the myristoylated protein. Source: prepared by the author.

5. Discussion

GRASPs are peripheral membrane proteins whose mechanism of anchoring, despite still lacking a detailed molecular understanding, has been proposed in general terms. Such mechanism, in most GRASPs, was suggested to involve the myristoylation of Gly2 of the GRASP domain along with the participation of a partner protein [48]. The crystal structures obtained so far for the GRASP domains [38], [49] were determined using protein constructions that lacked the myristoylation. Therefore, the description of this lipidation in the anchoring process has been somewhat limited. Due to its relevance in the functional cycle of GRASPs, it is still an issue that deserves more attention for a better understanding of the extensively discussed GRASP oligomerization [48].

Despite the plasticity of GRASPs in terms of structural organization, which includes the formation of dimers and fibrillar structures [88], [93], DGRASPs in solution have shown to be predominantly monomers [51], [52]. Furthermore, neutron reflection experiments suggested a restriction of the myr-DGRASP55 anchored in lipid membranes, affecting the potential of myr-DGRASP55 for self-interaction. Here, we explored the effects of myristoylation in one of the human GRASPs (GRASP55) and how this post-translational modification affects the protein structural behavior and its interaction with lipid membranes.

A successful myristoylation strategy that can be implemented during the heterologous expression of the protein in bacteria is a crucial step to obtain information on GRASP in scenarios that are more closely related to those found in the cell. Our myristoylation protocol was adapted from previous reports [75], [76]. The success in lipidating the DGRASP55 was assessed by different methods, as seen in Figure 9 and subsection 4.4. Several myristoylated proteins were already shown to utilize a controlled mechanism for binding to the membranes. These mechanisms can be represented by the interaction between hydrophobic residues, negatively charged residues, and co- and post-translational modifications [94]. For example, the Golgi-localized ARF1 (ADP ribosylation factor-1) [66] requires the presence of GTP for membrane binding [70], and Recoverin relies on a calcium-mediated conformational change to expose its myristoyl moiety [71], [72]. Our results (**Figures 9** and **10**B) indicate that DGRASP55 has its

myristoyl group already exposed to the solvent, therefore requiring the use of detergent to solubilize the myristoylated protein.

Once the myristoylation of DGRASP55 was successfully achieved, we further explored the effects of this post-translational modification on the protein's biophysical properties using a combination of experimental and computational methods. Our CD data measured in the far-UV range (Figure **11**) showed that the presence of the myristoyl moiety and the detergent molecules resulted in no changes to the overall protein's secondary structure, which suggests DGRASP55 would maintain its spatial organization upon myristoylation. On the other hand, alterations in the vicinity of the aromatic residues were seen in our near-UV CD data (**Figure 13**A), which indicates that local rearrangements would be expected upon interaction with the Golgi or other functionally relevant membranes. Another significant alteration introduced by the myristoyl group and the detergent micelles was seen in the thermal unfolding of DGRASP55 (**Figure 12**), which yielded different behavior upon temperature increasing. Myristoylation of proteins where the myristoyl is involved in protein-protein interactions showed increased stability [67], [95], [96]. For example, the myristoylation of human insulin induces structural effects that result in stable hexamers [69]. Myristoylation can also increase protein stability by inserting the lipid moiety into a hydrophobic pocket, such as observed in forming a recognition motif in the phosphorylation site of protein kinase A [95].

On the other hand, myristoylated proteins showed a decrease in solubility [67], [97], and in enthalpy of unfolding [98] compared with its non-myristoylated version. In the case of myr-DGRASP55 and DGRASP55, the presence of the myristoyl chain and the detergent yielded different thermal unfolding profiles (**Figure 12**). The myr-DGRASP55 protein had its far-UV CD spectrum unchanged as the temperature was raised, suggesting that myristoylation increased DGRASP55 stability.

The aforementioned changes in the local environment around the aromatic residues were also assessed by fluorescence and molecular dynamics simulations. More specifically, using steady-state fluorescence, the accessibility of the Trp residues present in DGRASP55 to a water-soluble quencher was measured. The lower Stern-Volmer

constant obtained for myr-DGRASP55, compared to its non-myristoylated form (**Figure 13**B), can be an effect of the self-association profile observed by size exclusion chromatography (SEC) (**Figure 10**A). In the non-myristoylated protein, the movement of that residue was not restricted by the myristoyl anchoring to the membrane, thus keeping it readily accessible to the quenching agent. In the experimental conditions, the solubilization of the myristoyl moiety by the detergent molecules that reduced quencher accessibility likely played a similar role to the anchoring in the lipid bilayer, which would also reduce tryptophan residues exposure due to its proximity to the membrane surface. The differences in near-UV CD data (**Figure 13**A) observed in the comparison of both protein versions can be explained by the differences in the microenvironment of the aromatic residues (Tyr16, Tyr165, Phe206) shown in **Figure 20**D. These differences arose because the residues located at the interface of the myristoyl region with the membrane-mimicking micellar surface were less water-accessible, as inferred by our SASA data (**Figures 22-26**), when compared with the same positions in the DGRASP55, which did not seem to interact with the lipid bilayer as inferred by our LEMSA data (subsection 4.4) and MD data (**Figure 20**B).

Moreover, we identified specific regions containing residues in contact (distance < 0.3 nm) with the lipid bilayer surface (**Figure 27**). The higher frequency of charged residues contacts (**Table 4**) was a characteristic also observed in our MD data. Based on the residues network in contact with phospholipids, we suggest that the final protein orientation in the simulations is favored by electrostatic interactions involving specific regions, such as salt bridges (**Figure 28**) and hydrogen bonds (**Figure 29**). A recent study using a DNA-based voltmeter found a high resting membrane potential measured at the *trans*-Golgi network, with a positively charged lumen [99]. Despite the dynamics of the Golgi membrane surface potential depends on several factors, for example, the influence of Na^+/K^+ ATPases, the charged membrane surface possibly impacts the interaction between phospholipids and residues mentioned above (regions 43 to 45 (Asn43, Gly44 and Ser45), 60 to 67 (Ala60, Asn61, Val62, Glu63, Lys64, Pro65, and Lys67) and 80 to 82 (Glu80 and Ser82)) (**Figure 27**B and **Figure 27**D).

In *in vivo* studies, GRASP55 was found in the endoplasmic reticulum under cell stress [34]. This relocalization of an anchored protein likely required a membrane dissociation that would involve the myristoylated N-terminal region. Although our data indicated the solvent exposure of the myristoyl moiety, the variety of specific interactions of the full-length myr-GRASP55 could still probably include the need for a myristoyl switch, a feature observed in several myristoylated proteins as a mechanism to expose the initially sequestered myristoyl chain upon the onset of specific conditions (MARCKS [64], Recoverin [71], [72], ARF1 [66]). Finally, GRASPs are the most phosphorylated Golgi proteins during mitosis [100], resulting in GRASP dimers disassembly and cisternae unstacking. This indicates the relevance of including phosphorylation in future studies involving myristoylated GRASPs and its role in the transition of the protein from the Golgi to other cell locations.

6. Conclusions and future perspectives

The biophysical properties of the myr-DGRASP55 are significantly different compared to the non-myristoylated protein. The myristoylation rendered a protein that is less soluble and more thermally stable. On the other hand, an explanation for the differences observed between these proteins in size-exclusion chromatography might be a consequence of protein self-association. Although there were no detectable differences in the secondary structure organization observed by the far-UV CD spectra, the lipidation altered the unfolding process monitored via the temperature dependence of the far-UV CD spectra. Additionally, we searched for a more detailed description of the membrane interaction mechanisms through molecular dynamics simulations and lipid electrophoretic mobility assays, confirming that myristoylation is essential for GRASP domain anchoring into lipid membranes or detergent micelles. Furthermore, we found that a coupled mechanism of binding is responsible for the restricted configuration of GRASP55 in membranes, and this is achieved without the need of a golgin partner or a mimetic of it.

The myristoylation of one of the two domains of the full-length GRASP55 resulted in interesting properties. It encouraged us to search for a possible role of the SPR domain in myristoylated GRASP membrane interaction. As mentioned before, since myristoylation is an irreversible lipidation, myristoylated proteins utilize switching mechanisms controlled by several properties such as charge, hydrophobicity, or ligand interaction. It was also shown that phosphorylation of GRASPs SPR domain induces membrane dissociation. Our results indicated that the GRASP domain itself could not utilize a switching mechanism. In future projects, we aim to explore the role of myristoylation in full-length GRASPs and how this impacts the lipid organization in the bilayer.

Since myristoylation is essential for GRASP's attachment to the membrane, the success in myristoylating DGRASP55 paves the way for future experiments in our group. It opens up the possibilities of finally exploring the GRASP-membrane interactions using the full-length lipidated protein. This will bring new insights into GRASP-membrane interaction and the effects of lipidation on the biophysical properties of these proteins.

7. References

[1] C. Viotti, “Unconventional Protein Secretion IN Series Editor,” vol. 1459, pp. 175–190, 2016, doi: 10.1007/978-1-4939-3804-9.

[2] X. Zhang *et al.*, “Hsp20 functions as a novel cardiokine in promoting angiogenesis via activation of VEGFR2,” *PLoS One*, vol. 7, no. 3, 2012, doi: 10.1371/journal.pone.0032765.

[3] H. Y. Gee, S. H. Noh, B. L. Tang, K. H. Kim, and M. G. Lee, “Rescue of ΔF508-CFTR trafficking via a GRASP-dependent unconventional secretion pathway,” *Cell*, vol. 146, no. 5, pp. 746–760, 2011, doi: 10.1016/j.cell.2011.07.021.

[4] T. A. Baldwin and H. L. Ostergaard, “The protein-tyrosine phosphatase CD45 reaches the cell surface via Golgi-dependent and -independent pathways,” *J. Biol. Chem.*, vol. 277, no. 52, pp. 50333–50340, 2002, doi: 10.1074/jbc.M209075200.

[5] H. Schotman, L. Karhinen, and C. Rabouille, “Integrins mediate their unconventional, mechanicalstress-induced secretion via RhoA and PINCH in Drosophila,” *J. Cell Sci.*, vol. 122, no. 15, pp. 2662–2672, 2009, doi: 10.1242/jcs.039347.

[6] C. Rabouille, V. Malhotra, and W. Nickel, “Diversity in unconventional protein secretion,” *J. Cell Sci.*, vol. 125, no. 22, pp. 5251–5255, Nov. 2012, doi: 10.1242/jcs.103630.

[7] J. Kim, H. Y. Gee, and M. G. Lee, “Unconventional protein secretion – new insights into the pathogenesis and therapeutic targets of human diseases,” *J. Cell Sci.*, vol. 131, no. 12, p. jcs213686, 2018, doi: 10.1242/jcs.213686.

[8] R. S. Polishchuk and A. A. Mironov, “Structural aspects of Golgi function,” *C. Cell. Mol. Life Sci*, vol. 61, pp. 146–158, 2004, doi: 10.1007/s00018-003-3353-8.

[9] M. A. Puthenveedu, C. Bachert, S. Puri, F. Lanni, and A. D. Linstedt, “GM130 and GRASP65-dependent lateral cisternal fusion allows uniform Golgi-enzyme distribution,” *Nat. Cell Biol.*, vol. 8, no. 3, pp. 238–248, Mar. 2006, doi: 10.1038/ncb1366.

[10] P. Stanley, “Golgi Glycosylation,” doi: 10.1101/cshperspect.a005199.

[11] G. Dick, L. K. Akslen-Hoel, F. Grøndahl, I. Kjos, and K. Prydz, “Proteoglycan Synthesis and Golgi Organization in Polarized Epithelial Cells,” *J. Histochem. Cytochem.*, vol. 60, no. 12, pp. 926–935, 2012, doi: 10.1369/0022155412461256.

[12] R. W. H. Lee and W. B. Huttner, “(Glu62,Ala30,Tyr8)(n) serves as high-affinity substrate for tyrosylprotein sulfotransferase: A Golgi enzyme,” *Proc. Natl. Acad. Sci. U. S. A.*, vol. 82, no. 18, pp. 6143–6147, 1985, doi: 10.1073/pnas.82.18.6143.

[13] J. M. Capasso, T. W. Keenan, C. Abeijon, and C. B. Hirschberg, “Mechanism of Phosphorylation in the Lumen of the Golgi Apparatus,” *J. Biol. Chem.*, vol. 264, no. 9, pp. 5233–5240, 1989, doi: 10.1016/s0021-9258(18)83723-1.

[14] X. Zhang and Y. Wang, “GRASPs in Golgi structure and function,” *Front. Cell Dev. Biol.*, vol. 3, no. JAN, pp. 1–8, 2016, doi: 10.3389/fcell.2015.00084.

[15] B. S. Donohoe *et al.*, “Cis-Golgi Cisternal Assembly and Biosynthetic Activation Occur Sequentially in Plants and Algae,” *Traffic*, vol. 14, no. 5, pp. 551–567, 2013, doi: 10.1111/tra.12052.

[16] F. A. Barr, M. Puype, J. Vandekerckhove, and G. Warren, “GRASP65, a protein involved in the stacking of Golgi cisternae,” *Cell*, vol. 91, no. 2, pp. 253–262, 1997, doi: 10.1016/S0092-8674(00)80407-9.

[17] J. Shorter, R. Watson, M. E. Giannakou, M. Clarke, G. Warren, and F. A. Barr, “GRASP55, a second mammalian GRASP protein involved in the stacking of Golgi cisternae in a cell-free system,” *EMBO J.*, vol. 18, no. 18, pp. 4949–4960, Sep. 1999, doi: 10.1093/emboj/18.18.4949.

[18] N. Nakamura *et al.*, “Characterization of a cis-Gol Matrix Protein, GM130,” *J. Cell Biol.*, vol. 131, no. 6, pp. 1715–1726, 1995.

[19] S. R. Pfeffer, “Constructing a Golgi complex,” *J. Cell Biol.*, vol. 155, no. 6, pp. 873–875, 2001, doi: 10.1083/jcb.200109095.

[20] Vangelis Kondylis; Kirsten M. Spoorendonk; Catherine Rabouille, “dGRASP Localization and Function in the Early Exocytic Pathway in Drosophila S2 Cells,” *Mol Biol Cell*, vol. 16, no. June, pp. 4061–4072, 2005, doi: 10.1091/mbc.E04–10–0938.

[21] R. Behnia, F. A. Barr, J. J. Flanagan, C. Barlowe, and S. Munro, “The yeast orthologue of GRASP65 forms a complex with a coiled-coil protein that contributes to ER to Golgi traffic,” *J. Cell Biol.*, vol. 176, no. 3, pp. 255–261, 2007, doi: 10.1083/jcb.200607151.

[22] N. S. Struck *et al.*, “Plasmodium falciparum possesses two GRASP proteins that are differentially targeted to the Golgi complex via a higher- and lower-eukaryote-

like mechanism," *J. Cell Sci.*, vol. 121, no. 13, pp. 2123–2129, 2008, doi: 10.1242/jcs.021154.

[23] P. Dupree and D. J. Sherrier, "The plant Golgi apparatus," *Biochim. Biophys. Acta - Mol. Cell Res.*, vol. 1404, no. 1–2, pp. 259–270, Aug. 1998, doi: 10.1016/S0167-4889(98)00061-5.

[24] Timothy N. Feinstein and Adam D. Linsted, "GRASP55 Regulates Golgi Ribbon Formation," *Mol. Biol. Cell*, vol. 19, no. July, pp. 2696–2707, 2008, doi: 10.1091/mbc.E07–11–1200.

[25] X. Zhang, L. Wang, B. Lak, J. Li, E. Jokitalo, and Y. Wang, "GRASP55 Senses Glucose Deprivation through O-GlcNAcylation to Promote Autophagosome-Lysosome Fusion," *Dev. Cell*, vol. 45, no. 2, pp. 245-261.e6, 2018, doi: 10.1016/j.devcel.2018.03.023.

[26] R. Grond *et al.*, "The function of GORASPs in Golgi apparatus organization in vivo," *J. Cell Biol.*, vol. 219, no. 9, 2020, doi: 10.1083/jcb.202004191062420 20c.

[27] M. E. Bekier *et al.*, "Knockout of the Golgi stacking proteins GRASP55 and GRASP65 impairs Golgi structure and function," *Mol. Biol. Cell*, 2017, doi: 10.1091/mbc.E17-02-0112.

[28] E. Ahat, Y. Xiang, X. Zhang, M. E. Bekier Ll, and Y. Wang, "GRASP depletion-mediated Golgi destruction decreases cell adhesion and migration via the reduction of α5β1 integrin," *Mol. Biol. Cell*, vol. 30, no. 6, pp. 766–777, 2019, doi: 10.1091/mbc.E18-07-0462.

[29] F. Giuliani, A. Grieve, and C. Rabouille, "Unconventional secretion: A stress on GRASP," *Curr. Opin. Cell Biol.*, vol. 23, no. 4, pp. 498–504, 2011, doi: 10.1016/j.ceb.2011.04.005.

[30] W. Nickel and C. Rabouille, "Mechanisms of regulated unconventional protein secretion," *Nat. Rev. Mol. Cell Biol.*, vol. 10, no. 2, pp. 148–155, 2009, doi: 10.1038/nrm2617.

[31] C. Rabouille, "Pathways of Unconventional Protein Secretion," *Trends Cell Biol.*, vol. 27, no. 3, pp. 230–240, 2017, doi: 10.1016/j.tcb.2016.11.007.

[32] M. Zhang, S. J. Kenny, L. Ge, K. Xu, and R. Schekman, "Translocation of interleukin-1β into a vesicle intermediate in autophagy-mediated secretion," *Elife*, vol. 4, no. NOVEMBER2015, Nov. 2015, doi: 10.7554/elife.11205.

[33] N. Dupont, S. Jiang, M. Pilli, W. Ornatowski, D. Bhattacharya, and V. Deretic, “Autophagy-based unconventional secretory pathway for extracellular delivery of IL-1β,” *EMBO J.*, vol. 30, no. 23, pp. 4701–4711, 2011, doi: 10.1038/emboj.2011.398.

[34] J. Kim *et al.*, “Monomerization and ER Relocalization of GRASP Is a Requisite for Unconventional Secretion of CFTR,” *Traffic*, vol. 17, no. 7, pp. 733–753, 2016, doi: 10.1111/tra.12403.

[35] T. Jarvela and A. D. Linstedt, “Golgi GRASPs: Moonlighting membrane tethers,” *Cell Health Cytoskelet.*, vol. 4, no. May 2012, pp. 37–47, 2012, doi: 10.2147/CHC.S21849.

[36] F. Hu, X. Shi, B. Li, X. Huang, X. Morelli, and N. Shi, “Structural basis for the interaction between the Golgi reassembly-stacking protein GRASP65 and the Golgi matrix protein GM130,” *J. Biol. Chem.*, vol. 290, no. 44, pp. 26373–26382, 2015, doi: 10.1074/jbc.M115.657940.

[37] J. Zhao, B. Li, X. Huang, X. Morelli, and N. Shi, “Structural basis for the interaction between Golgi reassembly-stacking protein GRASP55 and Golgin45,” *J. Biol. Chem.*, vol. 292, no. 7, pp. 2956–2965, 2017, doi: 10.1074/jbc.M116.765990.

[38] S. T. Truschel, D. Sengupta, A. Foote, A. Heroux, M. R. Macbeth, and A. D. Linstedt, “Structure of the membrane-tethering GRASP domain reveals a unique PDZ ligand interaction that mediates golgi biogenesis,” *J. Biol. Chem.*, vol. 286, no. 23, pp. 20125–20129, 2011, doi: 10.1074/jbc.C111.245324.

[39] E. Ahat, J. Li, and Y. Wang, “New Insights Into the Golgi Stacking Proteins,” *Front. Cell Dev. Biol.*, vol. 7, no. July, pp. 1–9, 2019, doi: 10.3389/fcell.2019.00131.

[40] L. Mendes, N. A. Fontana, S. T. Reddy, V. N. Uversky, and A. J. Costa-Filho, “The exquisite structural biophysics of the Golgi Reassembly and Stacking Proteins,” *Int. J. Biol. Macromol.*, vol. 164, pp. 3632–3644, 2020, doi: 10.1016/j.ijbiomac.2020.08.203.

[41] A. Cartier-Michaud *et al.*, “Genetic, structural, and chemical insights into the dual function of GRASP55 in germ cell Golgi remodeling and JAM-C polarized localization during spermatogenesis,” *PLoS Genet.*, vol. 13, no. 6, pp. 1–28, 2017, doi: 10.1371/journal.pgen.1006803.

[42] F. A. Barr, C. Preisinger, R. Kopajtich, and R. Körner, “Golgi matrix proteins interact with p24 cargo receptors and aid their efficient retention in the Golgi apparatus,” *J. Cell Biol.*, vol. 155, no. 6, pp. 885–891, 2001, doi: 10.1083/jcb.200108102.

[43] A. Kuo, “Transmembrane transforming growth factor-alpha tethers to the PDZ domain-containing, Golgi membrane-associated protein p59/GRASP55,” *EMBO J.*, vol. 19, no. 23, pp. 6427–6439, Dec. 2000, doi: 10.1093/emboj/19.23.6427.

[44] M. F. Stein *et al.*, “CD83 and GRASP55 interact in human dendritic cells,” *Biochem. Biophys. Res. Commun.*, vol. 459, no. 1, pp. 42–48, May 2015, doi: 10.1016/j.bbrc.2015.02.057.

[45] C. Roghi, L. Jones, M. Gratian, W. R. English, and G. Murphy, “Golgi reassembly stacking protein 55 interacts with membrane-type (MT) 1-matrix metalloprotease (MMP) and furin and plays a role in the activation of the MT1-MMP zymogen,” *FEBS J.*, vol. 277, no. 15, pp. 3158–3175, Aug. 2010, doi: 10.1111/j.1742-4658.2010.07723.x.

[46] F. A. Barr, M. Puype, J. Vandekerckhove, and G. Warren, “GRASP65, a protein involved in the stacking of Golgi cisternae,” *Cell*, vol. 91, no. 2, pp. 253–262, Oct. 1997, doi: 10.1016/S0092-8674(00)80407-9.

[47] J. Shorter, R. Watson, M. E. Giannakou, M. Clarke, G. Warren, and F. A. Barr, “GRASP55, a second mammalian GRASP protein involved in the stacking of Golgi cisternae in a cell-free system,” *EMBO J.*, 1999, doi: 10.1093/emboj/18.18.4949.

[48] C. Rabouille and A. D. Linstedt, “GRASP: A multitasking tether,” *Frontiers in Cell and Developmental Biology*. 2016, doi: 10.3389/fcell.2016.00001.

[49] Y. Feng *et al.*, “Structural insight into golgi membrane stacking by GRASP65 and GRASP55 proteins,” *J. Biol. Chem.*, vol. 288, no. 39, pp. 28418–28427, 2013, doi: 10.1074/jbc.M113.478024.

[50] D. Sengupta and A. D. Linstedt, “Mitotic inhibition of GRASP65 organelle tethering involves polo-like kinase 1 (PLK1) phosphorylation proximate to an internal PDZ ligand,” *J. Biol. Chem.*, vol. 285, no. 51, pp. 39994–40003, 2010, doi: 10.1074/jbc.M110.189449.

[51] S. T. Truschel, M. Zhang, C. Bachert, M. R. Macbeth, and A. D. Linstedt, “Allosteric regulation of GRASP protein-dependent golgi membrane tethering by

mitotic phosphorylation," *J. Biol. Chem.*, vol. 287, no. 24, pp. 19870–19875, 2012, doi: 10.1074/jbc.M111.326256.

[52] X. Li, Y. Feng, and X. Liu, "Crystallization and preliminary crystallographic studies of GRASP65 GRASP domain from Rattus norvegicus," *Acta Crystallogr. Sect. F Struct. Biol. Cryst. Commun.*, vol. 69, no. 7, pp. 792–795, 2013, doi: 10.1107/S1744309113015583.

[53] M. J. Nadolski and M. E. Linder, "Protein lipidation," *FEBS J.*, vol. 274, no. 20, pp. 5202–5210, 2007, doi: 10.1111/j.1742-4658.2007.06056.x.

[54] P. T. Englund, "The structure and biosynthesis of glycosyl phosphatidylinositol protein anchors," *Annu. Rev. Biochem.*, vol. 62, pp. 121–138, 1993, doi: 10.1146/annurev.biochem.62.1.121.

[55] P. J. Casey, "Protein lipidation in cell signaling," *Science (80-.).*, vol. 268, no. 5208, pp. 221–225, 1995, doi: 10.1126/science.7716512.

[56] H. Jiang, X. Zhang, X. Chen, P. Aramsangtienchai, Z. Tong, and H. Lin, "Protein Lipidation: Occurrence, Mechanisms, Biological Functions, and Enabling Technologies," *Chem. Rev.*, vol. 118, no. 3, pp. 919–988, 2018, doi: 10.1021/acs.chemrev.6b00750.

[57] J. A. Glomset, "The mechanism of the plasma cholesterol esterification reaction: Plasma fatty acid transferase," *BBA - Biochim. Biophys. Acta*, vol. 65, no. 1, pp. 128–135, 1962, doi: 10.1016/0006-3002(62)90156-7.

[58] D. A. Towler *et al.*, "Purification and characterization of yeast myristoyl CoA:protein N-myristoyltransferase," *Proc. Natl. Acad. Sci. U. S. A.*, vol. 84, no. 9, pp. 2708–2712, 1987, doi: 10.1073/pnas.84.9.2708.

[59] M. A. Perinpanayagam, E. Beauchamp, D. D. O. Martin, J. Y. W. Sim, M. C. Yap, and L. G. Berthiaume, "Regulation of co-and post-translational myristoylation of proteins during apoptosis: Interplay of N-myristoyltransferases and caspases," *FASEB J.*, vol. 27, no. 2, pp. 811–821, 2013, doi: 10.1096/fj.12-214924.

[60] F. Dyda, D. C. Klein, and A. B. Hickman, "Gcn5-r n-a :," pp. 81–103, 2000.

[61] T. Meinnel, C. Dian, and C. Giglione, "Myristoylation, an Ancient Protein Modification Mirroring Eukaryogenesis and Evolution," *Trends Biochem. Sci.*, vol. 45, no. 7, pp. 619–632, 2020, doi: 10.1016/j.tibs.2020.03.007.

[62] B. Boisson, C. Giglione, and T. Meinnel, "Unexpected Protein Families Including Cell Defense Components Feature in the N-Myristoylome of a Higher Eukaryote,"

J. Biol. Chem., vol. 278, no. 44, pp. 43418–43429, 2003, doi: 10.1074/jbc.M307321200.

[63] T. A. Farazi, G. Waksman, and J. I. Gordon, "The Biology and Enzymology of Protein N-Myristoylation," *J. Biol. Chem.*, vol. 276, no. 43, pp. 39501–39504, 2001, doi: 10.1074/jbc.R100042200.

[64] S. McLaughlin and A. Aderem, "The myristoyl-electrostatic switch: a modulator of reversible protein-membrane interactions," *Trends Biochem. Sci.*, vol. 20, no. 7, pp. 272–276, 1995, doi: 10.1016/S0968-0004(00)89042-8.

[65] C. T. Sigal, W. Zhou, C. A. Buser, S. McLaughlin, and M. D. Resh, "Amino-terminal basic residues of Src mediate membrane binding through electrostatic interaction with acidic phospholipids," *Proc. Natl. Acad. Sci. U. S. A.*, vol. 91, no. 25, pp. 12253–12257, 1994, doi: 10.1073/pnas.91.25.12253.

[66] Y. Liu, R. A. Kahn, and J. H. Prestegard, "Structure and Membrane Interaction of Myristoylated ARF1," *Structure*, vol. 17, no. 1, pp. 79–87, 2009, doi: 10.1016/j.str.2008.10.020.

[67] M. Geyer, C. E. Munte, J. Schorr, R. Kellner, and H. R. Kalbitzer, "Structure of the anchor-domain of myristoylated and non-myristoylated HIV-1 Nef protein," *J. Mol. Biol.*, vol. 289, no. 1, pp. 123–138, 1999, doi: 10.1006/jmbi.1999.2740.

[68] A. Borsatto, V. Marino, G. Abrusci, G. Lattanzi, and D. Dell'orco, "Effects of membrane and biological target on the structural and allosteric properties of recoverin: A computational approach," *Int. J. Mol. Sci.*, vol. 20, no. 20, 2019, doi: 10.3390/ijms20205009.

[69] H. B. Olsen and N. C. Kaarsholm, "Structural effects of protein lipidation as revealed by Lys(B29)-myristoyl, des(B30) insulin," *Biochemistry*, vol. 39, no. 39, pp. 11893–11900, 2000, doi: 10.1021/bi001201i.

[70] R. S. Haun, S. C. Tsai, R. Adamik, J. Moss, and M. Vaughan, "Effect of myristoylation on GTP-dependent binding of ADP-ribosylation factor to Golgi," *J. Biol. Chem.*, vol. 268, no. 10, pp. 7064–7068, 1993, doi: 10.1016/s0021-9258(18)53145-8.

[71] E. V. Olshevskaya, R. E. Hughes, J. B. Hurley, and A. M. Dizhoor, "Calcium binding, but not a calcium-myristoyl switch, controls the ability of guanylyl cyclase-activating protein GCAP-2 to regulate photoreceptor guanylyl cyclase," *J.*

Biol. Chem., vol. 272, no. 22, pp. 14327–14333, 1997, doi: 10.1074/jbc.272.22.14327.

[72] Š. Timr, R. Pleskot, J. Kadlec, M. Kohagen, A. Magarkar, and P. Jungwirth, "Membrane Binding of Recoverin: From Mechanistic Understanding to Biological Functionality," *ACS Cent. Sci.*, vol. 3, no. 8, pp. 868–874, 2017, doi: 10.1021/acscentsci.7b00210.

[73] T. Chida *et al.*, "N-myristoylation is essential for protein phosphatases PPM1A and PPM1B to dephosphorylate their physiological substrates in cells," *Biochem. J.*, vol. 449, no. 3, pp. 741–749, 2013, doi: 10.1042/BJ20121201.

[74] K. A. Neve, R. Qanbar, and M. Bouvier, "Role of palmitoylation/depalmitoylation reactions in G-protein-coupled receptor function," *Pharmacol. Ther.*, vol. 97, no. 1, pp. 1–33, 2003, doi: 10.1016/S0163-7258(02)00300-5.

[75] F. Heinrich, H. Nanda, H. Z. Goh, C. Bachert, M. Lösche, and A. D. Linstedt, "Myristoylation restricts orientation of the GRASP domain on membranes and promotes membrane tethering," *J. Biol. Chem.*, vol. 289, no. 14, pp. 9683–9691, Apr. 2014, doi: 10.1074/jbc.M113.543561.

[76] D. Sengupta, S. Truschel, C. Bachert, and A. D. Linstedt, "Organelle tethering by a homotypic PDZ interaction underlies formation of the Golgi membrane network," *J. Cell Biol.*, vol. 186, no. 1, pp. 41–55, 2009, doi: 10.1083/jcb.200902110.

[77] L. F. S. Mendes *et al.*, "The GRASP domain in golgi reassembly and stacking proteins: differences and similarities between lower and higher Eukaryotes," *FEBS J.*, vol. 286, no. 17, pp. 3340–3358, 2019, doi: 10.1111/febs.14869.

[78] V. K. Garg *et al.*, "MFPPI-Multi FASTA ProtParam Interface," *Bioinformation*, vol. 12, no. 2, p. 74, 2016, [Online]. Available: http://insilicogenomics.in/mfpcalc/mfppi.html.

[79] T. Schwede, J. Kopp, N. Guex, and M. C. Peitsch, "SWISS-MODEL: An automated protein homology-modeling server," *Nucleic Acids Res.*, vol. 31, no. 13, pp. 3381–3385, 2003, doi: 10.1093/nar/gkg520.

[80] S. Jo, T. Kim, V. G. Iyer, and W. Im, "CHARMM-GUI: A web-based graphical user interface for CHARMM," *J. Comput. Chem.*, vol. 29, no. 11, pp. 1859–1865, Aug. 2008, doi: 10.1002/jcc.20945.

[81] W. Humphrey *et al.*, “Scalable molecular dynamics on CPU and GPU architectures with NAMD,” *J. Mol. Graph.*, vol. 14, no. October 1995, pp. 33–38, 1996, doi: 10.1063/5.0014475.

[82] B. R. Brooks *et al.*, “CHARMM: The biomolecular simulation program,” *J. Comput. Chem.*, vol. 30, no. 10, pp. 1545–1614, Jul. 2009, doi: 10.1002/jcc.21287.

[83] D. R. Roe and T. E. Cheatham, “PTRAJ and CPPTRAJ: Software for Processing and Analysis of Molecular Dynamics Trajectory Data,” 2013, doi: 10.1021/ct400341p.

[84] R. C. et al. Wiegand, “The Candida albicans Myristoyl-CoA : Protein N-Myristoylatranferase Gene,” *J. Biol. Chem.*, vol. 267, pp. 8591–8598, 1992.

[85] W. P. Heal *et al.*, “Site-specific N-terminal labelling of proteins in vitro and in vivo using N-myristoyl transferase and bioorthogonal ligation chemistry,” *Chem. Commun.*, vol. 8, no. 4, pp. 480–482, 2002, doi: 10.1039/b716115h.

[86] J.-L. Rigaud, D. Levy, G. Mosser, and O. Lambert, “Detergent removal by non-polar polystyrene beads,” *Eur. Biophys. J.*, vol. 27, no. 4, pp. 305–319, 1998, doi: 10.1007/s002490050138.

[87] J. Zha, S. Weiler, K. J. Oh, M. C. Wei, and S. J. Korsmeyer, “Posttranslational N-myristoylation of BID as a molecular switch for targeting mitochondria and apoptosis,” *Science (80-.).*, vol. 290, no. 5497, pp. 1761–1765, 2000, doi: 10.1126/science.290.5497.1761.

[88] N. A. Fontana, R. Fonseca-Maldonado, L. F. S. Mendes, L. P. Meleiro, and A. J. Costa-Filho, “The yeast GRASP Grh1 displays a high polypeptide backbone mobility along with an amyloidogenic behavior,” *Sci. Rep.*, vol. 8, no. 1, pp. 1–14, 2018, doi: 10.1038/s41598-018-33955-1.

[89] G. E. Healthcare, “Size Exclusion Chromatography: Principles and Methods,” *GE Healthc.*, pp. 1–122, 2018, [Online]. Available: https://cdn.gelifesciences.com/dmm3bwsv3/AssetStream.aspx?mediaformatid=10061&destinationid=10016&assetid=11639.

[90] Z. Li and J. D. Hirst, “Quantitative first principles calculations of protein circular dichroism in the near-ultraviolet,” *Chem. Sci.*, vol. 8, no. 6, pp. 4318–4333, 2017, doi: 10.1039/c7sc00586e.

[91] L. B. Pérez Socas and E. E. Ambroggio, “The influence of myristoylation, liposome surface charge and nucleic acid interaction in the partition properties of

HIV-1 Gag-N-terminal peptides to membranes," *Biochim. Biophys. Acta - Biomembr.*, vol. 1862, no. 11, p. 183421, 2020, doi: 10.1016/j.bbamem.2020.183421.

[92] M. D. Resh, "Fatty acylation of proteins: New insights into membrane targeting of myristoylated and palmitoylated proteins," *Biochim. Biophys. Acta - Mol. Cell Res.*, vol. 1451, no. 1, pp. 1–16, 1999, doi: 10.1016/S0167-4889(99)00075-0.

[93] S. T. Reddy, V. N. Uversky, and A. J. Costa-Filho, "Nucleation-dependent amyloid fibrillation of human GRASP55 in aqueous solution," *Eur. Biophys. J.*, vol. 49, no. 2, pp. 133–143, 2020, doi: 10.1007/s00249-019-01419-7.

[94] A. M. Whited and A. Johs, "The interactions of peripheral membrane proteins with biological membranes," *Chem. Phys. Lipids*, vol. 192, pp. 51–59, 2015, doi: 10.1016/j.chemphyslip.2015.07.015.

[95] J. M. Sowadski, C. A. Ellis, and Madhusudan, "Detergent binding to unmyristylated protein kinase A - Structural implications for the role of myristate," *Journal of Bioenergetics and Biomembranes*, vol. 28, no. 1. pp. 7–12, 1996, doi: 10.1007/BF02150673.

[96] D. Muralidhar *et al.*, "Equilibrium Unfolding of Neuronal Calcium Sensor-1 N-TERMINAL MYRISTOYLATION INFLUENCES UNFOLDING AND REDUCES PROTEIN STIFFENING IN THE PRESENCE OF CALCIUM*," 2005, doi: 10.1074/jbc.M414243200.

[97] L. Berthiaume and M. D. Resh, "Biochemical characterization of a palmitoyl acyltransferase activity that palmitoylates myristoylated proteins," *J. Biol. Chem.*, vol. 270, no. 38, pp. 22399–22405, 1995, doi: 10.1074/jbc.270.38.22399.

[98] T. Schröder, H. Lilie, and C. Lange, "The myristoylation of guanylate cyclase-activating protein-2 causes an increase in thermodynamic stability in the presence but not in the absence of Ca2+," *Protein Sci.*, vol. 20, no. 7, pp. 1155–1165, 2011, doi: 10.1002/pro.643.

[99] A. Saminathan *et al.*, "A DNA-based voltmeter for organelles," *Nat. Nanotechnol.*, vol. 16, no. 1, pp. 96–103, 2021, doi: 10.1038/s41565-020-00784-1.

[100] Y. Wang, J. Seemann, M. Pypaert, J. Shorter, and G. Warren, "A direct role for GRASP65 as a mitotically regulated Golgi stacking factor," *EMBO J.*, vol. 22, no. 13, pp. 3279–3290, 2003, doi: 10.1093/emboj/cdg317.